Shahid Chamran University of Ahvaz

Journal of

Applied and Computational Mechanics

Research Paper

Enhancing the Performance and Coordination of Multi-Point Absorbers for Efficient Power Generation and Grid Synchronization Control

Ali Alnujaie[1] , Abderrahmane Berkani[2] , Karim Negadi[2] , Lazreg Hadji[3] , Mofareh Hassan Ghazwani[1]

[1] Mechanical Engineering Department, Faculty of Engineering, Jazan University, P.O. Box 114, Jazan, 45142, Kingdom of Saudi Arabia,
Email: aalnajei@jazanu.edu.sa (A.A.); ghazwani@jazanu.edu.sa (M.H.G.)

[2] L2GEGI Laboratory, Department of Electrical Engineering, Faculty of Applied Science, University of Tiaret, BP 78 Zaaroura, 14000, Tiaret, Algeria,
Email: abderrahmane.berkani@univ-tiaret.dz (A.B.); karim.negadi@univ-tiaret.dz (K.N.)

[3] Department of Civil Engineering, University of Tiaret, BP 78 Zaaroura, Tiaret, 4000, Algeria, Email: lazreg.hadji@univ-tiaret.dz

Abstract. The increased use of renewable energy in modern power grids has led to a demand for innovative technologies that can efficiently harness intermittent energy sources. Multi-Point Absorber (MPA) systems have emerged as a promising solution for capturing wave and tidal energy sustainably. This study focuses on developing advanced control strategies for MPA systems to improve their performance and coordination in power generation and grid integration for both AC and DC networks. The research begins with a comprehensive review of MPA technologies, highlighting their challenges and opportunities. It then explores the development of control algorithms that dynamically adjust MPA parameters in real-time, optimizing energy extraction efficiency. The paper also addresses the crucial aspect of grid integration, investigating power electronics interfaces and synchronization techniques to enhance grid stability. Additionally, bidirectional power flow capabilities are discussed, enabling functions like frequency regulation and voltage control. The novelty of this work lies in the development of adaptive control algorithms for MPA systems, surpassing previous efforts by incorporating real-time data for parameter adjustments. The study demonstrates the effectiveness of these advanced control strategies through simulations and implementation, evaluating energy conversion efficiency, grid compatibility, and system reliability across various conditions compared to conventional methods. The results emphasize the significance of bidirectional power flow capabilities in achieving enhanced functionality, such as frequency regulation and voltage control. This paper provides valuable insights into optimizing MPA systems, showcasing their potential to revolutionize sustainable energy capture and integration into modern power grids.

Keywords: Multi-Point Absorbers, MPPT Control, Grid integration, Synchronization, Power converter, Sustainable energy.

1. Introduction

In order to achieve a sustainable and environmentally responsible future, it is essential that renewable energy sources be incorporated into the global energy system. Wave and tidal energy among the varied variety of renewable energy sources offer special benefits due to their predictability and high energy density. A promising method for utilizing this enormous oceanic potential, Multi-Point Absorber (MPA) devices promise reliable and sustainable power generation. The effective use of these marine resources brings opportunities and difficulties as the world moves toward an energy paradigm that is centered on renewable resources.

Over the past few decades, researchers have worked to improve the extracted power from the point absorber WEC using analytical, computational, and physical approaches [1] suggested a formula based on the Morison equation to find a hydraulic system's maximum extractions under regular waves; nonetheless, the linear PTO and drag viscosity were the basis for these findings. The wave height reduction-based physical technique known as "wave height take-off" (WHTO) was utilized to compute the WEC's energy absorption [2]. A point-absorber device's ability to trap energy in both regular and irregular waves was examined in [2, 3].

In the context of power generation and grid integration, this work presents a thorough investigation into cutting-edge control algorithms designed to improve the performance and coordination of Multi-Point Absorber systems. In order to accommodate both alternating current (AC) and direct current (DC) electrical networks, the goal is to address the multidimensional complexity involved with MPAs. Our goal is to fully realize the potential of MPAs and smoothly integrate their power output into current electrical grids, so making a substantial contribution to the diversification and environmental friendliness of our energy sources.

Due to the fluctuation of the wave resource, the power output of wave energy devices is not optimal, and they cannot be conventionally connected directly to the grid. The issues involved in the grid integration process range from effective control of the power converters involved to power conditioning procedures. Some grid integration lessons learned from wind energy can be applied to the case of wave energy [4, 5]. Wave energy's ability to enter current grid networks will, however, be directly impacted by the impacts it will have on the system and the availability of technologies to address these effects [6].

The most recent MPA technologies are thoroughly evaluated at the outset of this study in order to identify their inherent benefits and the specific challenges that stand in the way of their wider application. To overcome these limitations, we develop and implement advanced control algorithms that are meticulously designed to significantly optimize the energy extraction efficiency of MPAs throughout the dynamic and usually unpredictable marine environment. These control systems use real-time data, such wave and tide patterns, to adaptively fine-tune operational settings. As a result, the system experiences less mechanical stress and produces more power [7].

The smooth connection to both the AC and DC electrical grids is another important feature of renewable energy integration that is covered in this study. This research investigates cutting-edge power electronics interfaces and grid synchronization methods in recognition of the diversity in power distribution networks around the world. Regardless of the current network configuration, these advances are essential for enabling MPA systems to actively contribute to grid stability, reliability, and performance improvement [8, 9].

In addition to improved grid integration, the research examines the bidirectional power flow capabilities incorporated into MPA systems. This capability, for example, empowers MPAs to carry out essential grid support functions like voltage management and frequency regulation, which enhances their standing as adaptive and flexible players in the evolving energy scene. We evaluate the efficacy and resilience of the suggested advanced control mechanisms for MPA systems through an extensive set of simulations validations. Performance indicators like energy conversion efficiency, compliance with grid integration, and system reliability are systematically assessed under various operational circumstances, allowing for direct comparisons with traditional control techniques.

This paper aims to provide a holistic framework for the development and deployment of advanced control systems tailored specifically to Multi-Point Absorber technology. These advancements hold the promise of significantly enhancing energy conversion efficiency and seamless grid integration across both AC and DC current networks. As we embark on this journey towards a more sustainable energy future, the innovations presented here will undoubtedly play a pivotal role in realizing the full potential of wave and tidal energy resources, paving the way for a greener and more resilient global energy landscape.

The reminder of the paper is organized as follows: The introduction starts off by giving a quick summary of the case study. The overview of multi-point absorber technology is included in section 2 as well. The configuration of the wave energy-based point absorber is provided in Section 3. The many wave-based energy generating processes are described in Section 4. Section 5 discusses the approaches for hydrodynamic modeling of the absorber point. Section 6 focuses on the physical modeling of the linear permanent magnet synchronous generator and heaving buoy-based point absorber components. A model control-based power generation is described in section 7. The simulation results and analyses are presented in Section 8. Section 9 concludes by summarizing the research's main findings and exploring potential directions for the future.

2. Multi-Point Absorber (MPA) Technology Overview

Multi-Point Absorber (MPA) technology represents a pioneering approach to harvesting renewable energy from ocean waves and tidal currents. It stands at the forefront of marine renewable energy solutions, offering the potential for consistent, sustainable, and environmentally friendly power generation. In this section, we provide an in-depth overview of MPA technology, exploring its key principles, components, advantages, and challenges [10].

It becomes clear that the successful integration of wave energy into the electrical grid strongly depends on the efficient coordination of multiple subsystems as we work to harness wave energy as a viable renewable resource [11]. These subsystems cover a wide range of technologies, such as power conversion systems, energy storage options, wave energy converters, and sophisticated control systems as shown in Fig. 1. Since it calls for both the separate subsystems' optimization and the smooth coordination of their operations, the interconnection of various parts is a crucial problem in the development of wave energy systems. The complexity of these subsystems and their complex interactions are explored in this essay, along with the major concerns and innovations needed to advance wave energy as a dependable and sustainable addition to our energy mix.

A point absorber is a type of wave energy converter that captures energy from ocean waves. Modeling a point absorber involves both electrical and hydrodynamic aspects. Here are the key equations for modeling a point absorber:

A straightforward sketch can be used to demonstrate the concept and design of a Wave Energy Converter (WEC). The fundamental function of a WEC is to capture the kinetic and potential energy found in ocean waves and transform it into useful electrical power [12]. You may represent a buoyant structure that rides the waves in the sketch by showing how it rises and falls as the waves pass by. A mechanical linkage, frequently in the form of a piston or hydraulic system, is connected to this buoy and converts the vertical motion into mechanical motion as illustrate in Fig.3. The generator, which is pictured as a box with coils and magnets, receives this mechanical energy and uses it to generate electricity [13]. The generator is coupled to an electrical output that can either charge a battery-based local energy storage device or feed into the power grid. In order to maximize energy capture and adjust to changing wave conditions, the drawing can also include sensors and control systems. The fundamental idea is that a well-designed WEC system can convert wave motion into mechanical motion, and ultimately into electrical energy.
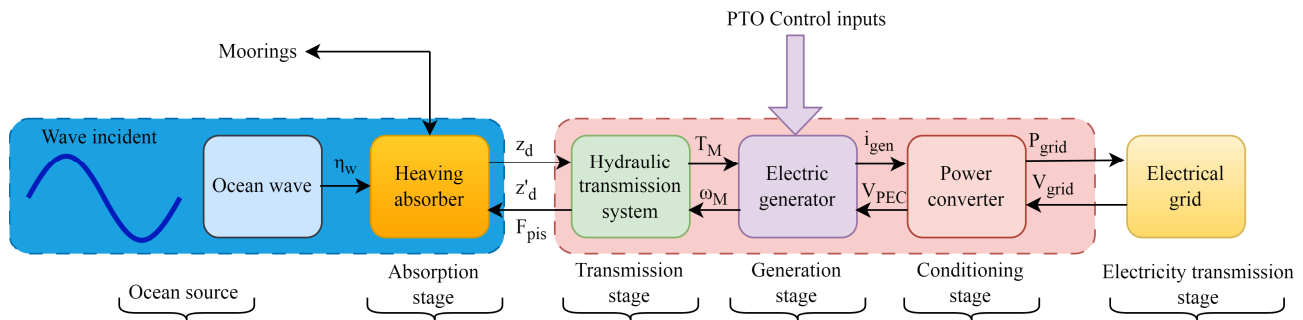

Fig. 1. The many subsystems involved in producing wave energy and its interconnection.

The equivalent circuit of a point absorber for marine energy conversion shown in Fig. 4 is a simplified electrical representation that captures the essential components and behaviors of the system. It typically consists of a Power Take-Off (PTO) component, which transforms the mechanical motion of the buoyant structure into electrical power by acting as a voltage source with an internal impedance [11]. To store and regulate the generated energy, energy storage components like capacitors and batteries are frequently used. Rectifiers and inverters may be included into the circuit depending on the required output. Control systems are essential for increasing power capture efficiency and guaranteeing smooth operation. The electrical load, in the end, stands for the things that use the power that is produced.

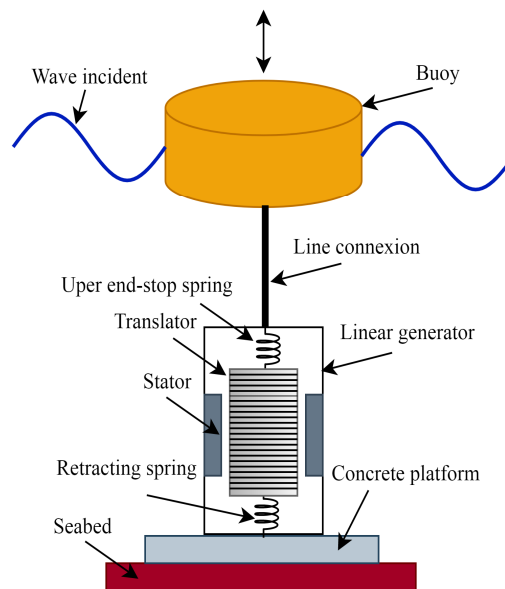**Fig. 2.** A common example of self-reacting a-body PAs is the OPT Power Buoy gadget [12].

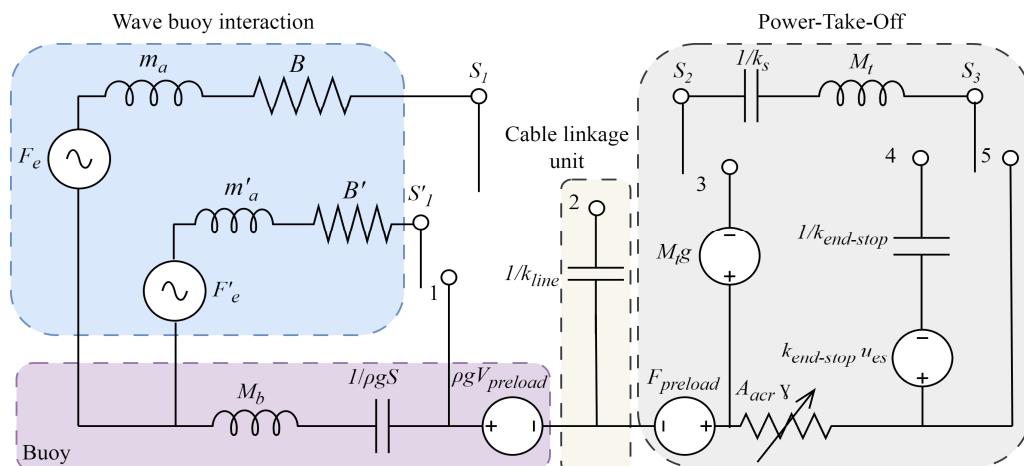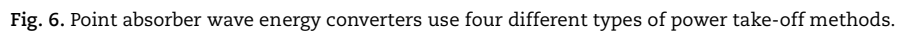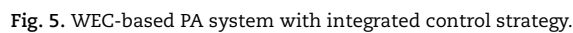**Fig. 3.** Principle and design of the WEC in a sketch.

Fig. 4. Equivalent circuit representation of marine energy point absorber.

Fig. 5. WEC-based PA system with integrated control strategy.

Fig. 6. Point absorber wave energy converters use four different types of power take-off methods.

3. Description of the Marine Conversion Chain

A point absorber, a linear permanent magnet synchronous generator (LPMSG), a diode rectifier, a DC-DC boost converter, and a two-level, three-phase voltage source inverter for grid connection make up the proposed WEC configuration, which is shown in Fig. 5. The grid-connected VSI is fed by the point absorber via current output dc/dc converter, which is arranged as a current source. To the shared dc-link, additional point absorber units with current output dc/dc converters may be connected in parallel [16]. The VSI uses voltage loop control to maintain consistent control of the dc-link voltage.

The grid inverter was implemented as a three-level NPC converter in both topologies. Only active power should be delivered to the grid, and the converter should keep the DC link's constant voltage V_{dc} at a predetermined level. The voltage-oriented control (VOC), in which the current component i_d is proportionate to the active power and the component i_q corresponds to the reactive power, was used to operate the master control system. The control system under test adopted a reactive power of zero ($i_q = 0$), which indicates that the grid current provided is in phase opposition to the grid voltage [17]. The set three-phase currents (i_{ga}, i_{gb}, i_{gc}) are created as in the generator converter employing a nonlinear three-level type regulator after transformation to a three-phase coordinate system.

4. A Point Absorber Mechanism

Power Take-Off (PTO) mechanisms are essential parts in a variety of applications where mechanical power needs to be transferred to or extracted from a prime mover or energy source for the completion of particular tasks [18]. They come in a variety of forms, each suited to particular uses and specifications. In this article, we go over four popular PTO mechanisms: hydraulic, mechanical, direct-drive, and novel or specialized PTOs.

In this study, we are interested in the third type direct drive PTO shown in Fig. 6.

Each mechanism illustrated in Fig. 6 has advantages and disadvantages and the choice of the appropriate topology depends on several geographical, economic and technical factors. Here is a brief description of each type:

4.1. Hydraulic PTOs

Pressurized fluids, mainly hydraulic oil, are used by hydraulic PTOs to transfer power. In order to transform mechanical energy into hydraulic pressure and vice versa, they need hydraulic pumps and motors. The applications of hydraulic PTOs are frequently used to drive winches, cranes, and various hydraulic systems in the construction, agricultural, and maritime industries. They are also frequently used in heavy machinery and industrial equipment.

4.2. Mechanical PTOs

Mechanical linkages, gears, and shafts are used in mechanical PTOs to transfer power. For engagement and disengagement, they frequently use clutches. Their field of application are the power auxiliary equipment like pumps, generators, or power take-offs for accessories, mechanical PTOs are frequently used in vehicles, including trucks and tractors.

4.3. Direct-drive PTOs

The goal of direct-drive PTOs is to convert mechanical energy directly into electrical power without the use of any intermediary conversion processes. They frequently employ prime mover-connected high-torque electric generators. To produce electricity more effectively, direct-drive PTOs are employed in a growing number of renewable energy systems, such as wind turbines and wave energy converters.

4.4. Alternative PTO systems

Its principle is to cutting-edge and distinctive PTOs that are specifically crafted for given purposes or challenges are referred to as innovative or specialized PTOs. Innovative technologies like magnetically connected PTOs, piezoelectric PTOs, or sophisticated energy collecting systems may be a part of these solutions. Its applications include energy harvesting in difficult or remote areas and the conversion of ocean energy, two fields that are just emerging. These PTOs are designed to meet specific needs.

Whether it's for moving auxiliary equipment in automobiles, producing electricity from renewable sources, powering hydraulic systems, or satisfying specific energy harvesting requirements, each of these PTO devices plays a critical role in effectively transmitting power [19]. The variety and adaptability of power take-off technologies are highlighted by the fact that the selection of a PTO mechanism is influenced by elements such as application, efficiency, and environmental circumstances.

5. Hydrodynamic Methods Applied to PA Modelling

Hydrodynamic modeling for wave energy devices like Point Absorber (PA) systems involves simulating and analyzing the motion and interaction of the device with the surrounding water environment [20]. These models are crucial for understanding how PA devices respond to wave forces, predicting their performance, and optimizing their design. Here are some common techniques used for hydrodynamic modeling of PA devices:

5.1. Potential flow theory

Potential flow models are often used for initial assessments of PA devices. These models assume irrotational flow (no vorticity) and can provide simplified estimates of device motion and response to wave forces. The linear potential flow theory is a common starting point for analyzing PA behavior.

5.2. Boundary element method (BEM)

BEM is a numerical technique used to solve potential flow problems more accurately. It discretizes the surfaces of the PA device and the water domain into elements, allowing for the accurate modeling of the complex geometry and wave interactions. BEM can handle non-linearities and is suitable for both regular and irregular wave conditions.

5.3. Computational fluid dynamics (CFD)

CFD simulations provide a higher level of detail by solving the Navier-Stokes equations to account for fluid viscosity and turbulence. While computationally more intensive, CFD can capture intricate flow patterns around PA devices, making it suitable for analyzing non-linear effects and complex geometries.

5.4. Linear frequency-domain analysis

This technique is used to analyze the frequency-domain response of PA devices to irregular waves. Linearization is applied to wave excitation and device response, which simplifies calculations while still providing valuable insights into device behavior.

5.5. Time-domain analysis

Time-domain simulations involve solving the equations of motion for the PA device over time. This approach accounts for non-linear effects, including wave steepness, device motion, and energy capture. Time-domain analysis is essential for understanding dynamic behavior and can be coupled with CFD or BEM for accuracy.

5.6. Numerical wave tank experiments

In addition to numerical modeling, physical experiments in wave tanks can validate and complement modeling efforts. These experiments involve scaled-down PA device prototypes and provide real-world data for comparison with simulations.

5.7. Frequency response analysis

This technique focuses on the frequency response of the PA device to harmonic excitations. It helps identify natural frequencies, resonances, and modes of vibration, which are crucial for optimizing control strategies.
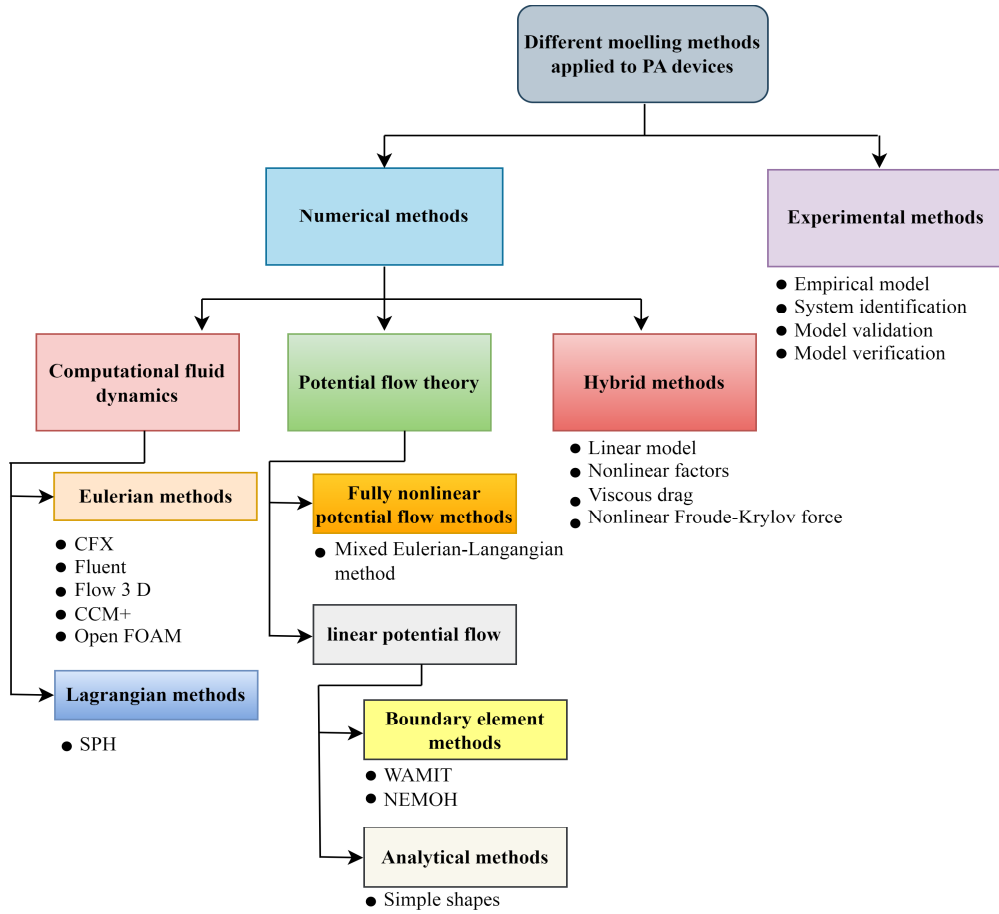
Fig. 7. The techniques for hydrodynamic modeling used with PA devices.

5.8. Dynamic response analysis

This involves assessing the dynamic response of PA devices under various sea conditions, including extreme wave scenarios. It can help ensure the structural integrity of the device and evaluate its performance over a wide range of conditions.

Effective hydrodynamic modeling of PA devices requires a combination of these techniques, depending on the specific research goals and the complexity of the device design. Researchers typically use a stepwise approach, starting with simplified models and gradually refining them as the understanding of the device's behavior improves.

Figure 7 gives a brief summary of the several hydrodynamic modeling approaches. These techniques are essential for comprehending the intricate dynamics of fluid flow in various natural and artificial systems [21].

The Navier-Stokes equations, the foundation of fluid mechanics, are one of the many mathematical and computational methods they cover. These equations are frequently written as [22]:

$$\frac{\partial \rho_\omega}{\partial t} + \nabla(\rho_\omega v) = 0 \tag{1}$$

$$\frac{\partial v}{\partial t} + (v\nabla)v = -\frac{1}{\rho_\omega}\nabla p_f + F + \frac{\mu}{\rho_\omega}\nabla^2 v \tag{2}$$

where:

$v(x, y, z)$: is the fluid flow velocity vector.

p_f : is the pressure field.

F : is the external force per unit mass.

μ : is the fluid viscosity.

Equations (1) and (2), however, cannot be resolved analytically; hence, numerical discretisation is required to arrive at a solution. The full set of Navier-Stokes equations must now be implemented using computer codes. The choice amongst the various methods is determined by the phenomenon that needs to be mimicked, the computing power of our computer, and/or the necessity for fidelity. Wave tank studies or open water tests can be carried out in NWTs in the case of wave energy [23]. For years, fluid-body interaction analysis in offshore and ocean engineering has used these simulations.

6. Modelling of Multi-point Absorber-based LPMSG

6.1. Hydrodynamics model of PA

Its methodology for PA hydrodynamic modeling is the same as that of the other kinds of WEC devices. This paper simply provides a basic overview of the PA hydrodynamic modeling because there are many works that deal with WEC hydrodynamic modeling [24].

Wave equation: The motion of the point absorber is influenced by the incoming wave motion. The wave elevation can be described by the linear wave theory equation [25]:

$$\eta(x,t) = A\cos(kx - \omega t)$$ (3)

where:

η : is the wave elevation.

A : is the wave amplitude.

k : is the wave number.

ω : is the angular frequency.

x : is the horizontal position.

t : is time.

Particle velocity: the particle velocity of the water particles beneath the absorber is given by:

$$u(x,t) = -\frac{A\omega}{k}\sin(kx - \omega t)$$ (4)

This velocity is important for estimating the kinetic energy of the incident waves. Buoyancy Force: The buoyancy force acting on the point absorber can be calculated using Archimedes' principle [23]:

$$F_b = \rho_\omega gV$$ (5)

where:

F_b : is the buoyancy force.

ρ_ω : is the density of water.

g : is the acceleration due to gravity.

V : is the volume displaced by the point absorber.

Power Capture: The electrical power captured by the point absorber can be calculated using the equation:

$$P_e = \frac{1}{2}\rho_\omega gVH_sC_dv^3P_g$$ (6)

where:

P_e : is the electrical power output.

H_s : is the significant wave height.

C_d : is the power capture coefficient.

v : is the relative velocity between the absorber and the waves.

P_g : is the generator efficiency.

Time domain models are necessary to analyze the device's nonlinear effects. Without describing how they interact, Eq. (7) captures all the forces acting on a wave energy device.

Then, Newton's second law is taken into account for a floating body that is solely constrained in heave motion. It states that the body's total force, F_{net}, is equal to its mass times the translational acceleration (moments are not treated here but follow the same rules [27]:

$$F_{net} = m\frac{d^2z(t)}{dt^2} = F_g(t) + F_{FK}(t) + F_{rad}(t) + F_{res}(t) + F_{PTO}(t) + F_{spring}(t) + F_{add}(t)$$ (7)

where:

F_{net} : is the sum of the forces acting on the buoy (N)

m : is the mass of the Point Absorber (kg)

$z(t)$: is the vertical displacement of the point absorber as a function of time (m)

g : is the acceleration due to gravity (m/s²)

$F_g(t)$: is the gravity force (N)

$F_{FK}(t)$: is the Froude-Krylov force (N)

$F_{rad}(t)$: is the radiation force (N)

$F_{res}(t)$: is the viscous force (N)

$F_{PTO}(t)$: is the PTO force (N)

$F_{spring}(t)$: is the mooring force (N)

$F_{add}(t)$: is the additional force (N), and F_{add} is any other force, such as drift, wind, tidal, or other body-water interactions, acting on the structure.

Gravity force: the force due to gravity acting on the point absorber:

$$F_g(t) = -mg$$ (8)

Froude-Krylov Force: the hydrodynamic force due to the motion of the point absorber. It depends on the acceleration of the point absorber:

$$F_{FK}(t) = -m\frac{d^2z(t)}{dt^2}$$ (9)

Radiation Force: the force due to the radiated waves from the motion of the point absorber. It also depends on the absorber's motion. As was already mentioned, the radiation force, or F_{rad}, drains energy from the system. Because of this, F_{rad} is acting as a damper, and as a result, it is proportional to the floater's velocity as follows:

$$F_{rad}(t) = -b\dot{z}(t)$$ (10)

where:

$\dot{b}$: is a radiation damping coefficient (kg/s)
$\dot{z}$: is the first-time derivative of the vertical displacement of the buoy, i.e. the velocity [m/s].

The restoring force, F_{res} according to Archimedes law of buoyancy, is taken proportional to the vertical displacement of the buoy according to:

$$F_{ras}(t) = -cz(t) \tag{11}$$

where:

c : is a restoring coefficient (kg/s^2)
z : is the vertical displacement of the buoy (m)

Power Take-Off (PTO) force: the force generated by the PTO system, which extracts energy from the motion of the point absorber. Like the restorative force F_{res}, radiation force F_{rad}, mechanical spring force F_{spring}, and PTO damping force (F_{PTO}), these forces are generated by:

$$F_{Spring}(t) = -k_{SP}z(t) \tag{12}$$

$$F_{PTO}(t) = -\beta\dot{z}(t) \tag{13}$$

where:

k_{sp} : is a mechanical spring coefficient (kg/s^2)
β : is the PTO damping coefficient (kg/s).

Additional force: any other forces that may act on the point absorber, such as drift, wind, tidal forces, or other body-water interactions. The added mass force, F_{add}, acts in addition to the absolute mass of the buoy, as suggested by its name, and is therefore taken to be proportional to the floater's acceleration as follows:

$$F_{add}(t) = -a\ddot{z}(t) \tag{14}$$

where:

a : is an added mass coefficient (kg)
$\ddot{z}$: is the second time derivative of the buoy's vertical displacement z(t), i.e., the acceleration (m/s^2)

Solving Eq. (7) of motion with appropriate numerical methods and considering the specific characteristics and design of the point absorber will provide insights into its behavior and energy conversion performance.

The different forces exerted on the mass of the point absorber in a terrestrial reference frame are represented in Fig. 8 in the part which contains the hydrodynamic chain. In the same figure we observe the connection of the electrical chain with the hydrodynamic one [28].

6.2. Linear permanent magnet synchronous generator model

A Linear Permanent Magnet Synchronous Generator (LPMSG) is a machine that produces electricity by revolving a coil of windings in relation to a permanent magnet field. Although it is set up for linear motion rather than rotating motion, it functions according to the same principles as a conventional Permanent Magnet Synchronous Generator (PMSG). An LPMSG simple model is provided below [29]:
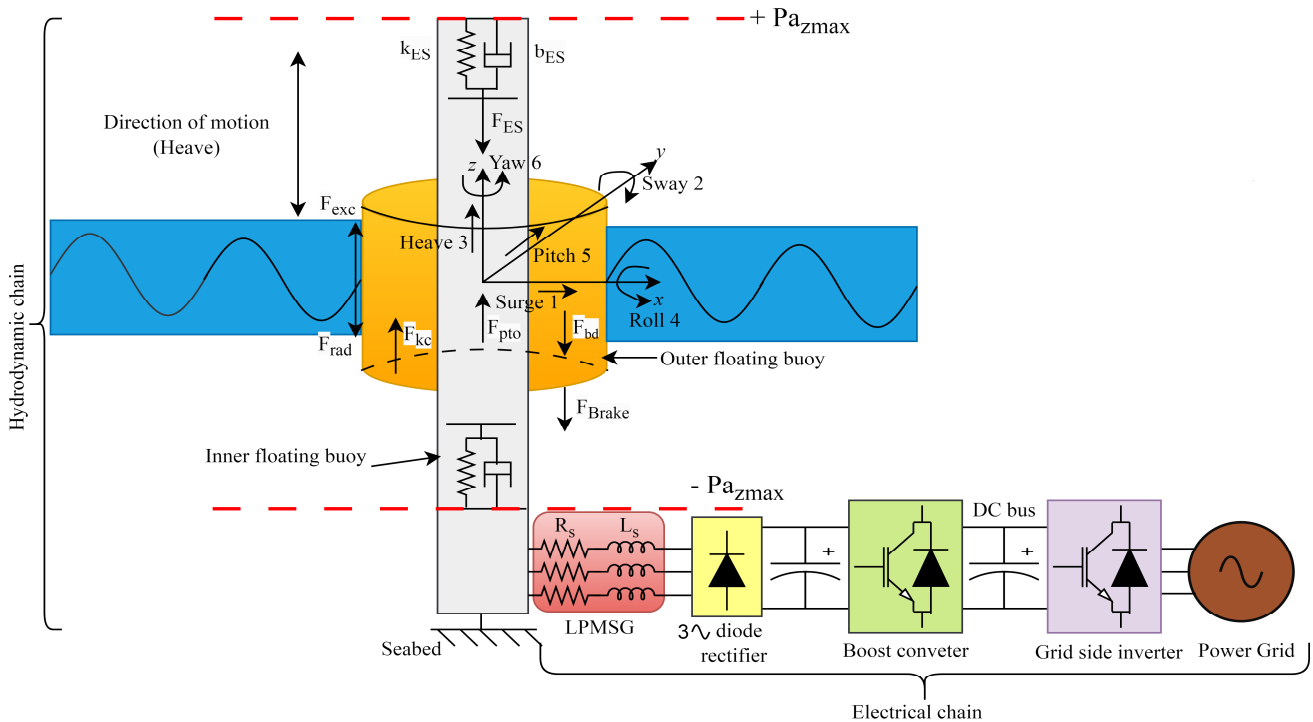

Fig. 8. The point absorber wave energy conversion based the element of a hydrodynamic and electrical chain.

$$v_d(t) = Ri_d(t) + \frac{d\psi_d(t)}{dt} - \omega_e(t)\psi_q(t) \tag{15}$$

$$v_q(t) = Ri_q(t) + \frac{d\psi_q(t)}{dt} + \omega_e(t)\psi_d(t) \tag{16}$$

where the voltages, currents, and magnetic flux connections in the direct- and quadrature-axis, respectively, are denoted by v_d, v_q, i_d, i_q, ψ_d, and ψ_q, R stands for electrical resistance per phase, while ω_e stands for angular electrical speed.

The flux wave moves axially in linear machines, but in the reference frame it generates an electrical speed v_e that is comparable to the electrical speed ω_e as in rotary machines. This speed is also stated in linear topologies in terms of radians per second (rad/s), and it can be calculated by:

$$v_e(t) = \frac{p\pi}{\tau_p}v_m(t) \tag{17}$$

where:

p : is the number of pole pairs,

v_m : is the mechanical linear speed (m/s).

As a result, the equations for linear machines can be explained similarly, or in terms that are analogous to Eqs. (15) and (16) as:

$$v_d(t) = Ri_d(t) + \frac{d\psi_d(t)}{dt} - v_e(t)\psi_q(t) \tag{18}$$

$$v_d(t) = Ri_d(t) + \frac{d\psi_d(t)}{dt} - v_e(t)\psi_q(t) \tag{19}$$

in which $\psi_q(t) = L_q i_q(t)$ and $\psi_d(t) = L_d i_d(t) + \psi_{mg}$, respectively, are the formulas for the d- and q-axis magnetic flux linkages. L_d, L_q, and ψ_{mg} stand for the direct-axis inductance, quadrature-axis inductance, and the fundamental component of magnetic flux linkage per pole produced by the PM arrays.

Equations (18) and (19) can therefore be rewritten as:

$$\frac{di_d(t)}{dt} = \frac{v_d(t) - Ri_d(t) + v_e(t)L_q i_q(t)}{L_d} \tag{20}$$

$$\frac{di_q(t)}{dt} = \frac{v_q(t) - Ri_q(t) - v_e(t)L_d i_d(t) - v_e(t)\psi_{PM}}{L_q} \tag{21}$$

The dynamics of currents and voltages in an LPMSM's synchronous reference frame are represented by equations (20) and (21). Typically, a rotary machine's torque equation is:

$$T(t) = J\frac{d\omega_m(t)}{dt} + B_v\omega_m(t) + T_L(t) \tag{22}$$

where T, J, B_v, T_L and ω_m stand for the electromagnetic torque, moment of inertia, damping coefficient, load torque, and angular speed produced by the motor, respectively.

A LPMSM's mechanical equation is so as follows:

$$F(t) = m\frac{dv_m(t)}{dt} + B_v v_m(t) + F_L(t) \tag{23}$$

where, respectively, F, m, and F_L stand for the electromagnetic force generated by the linear machine, the moving mass, and the load force. The torque on a rotary machine is comparable to force in the linear case, as can be observed from (22) and (23). Given its electric, magnetic, and geometrical characteristics, an LPMSM's electromagnetic force can be calculated as follows:

$$F(t) = \frac{3}{2}\frac{\pi}{\tau_p}p\left(\psi_{PM}i_q(t) - \left(L_d - L_q\right)i_d(t)i_q(t)\right) \tag{24}$$
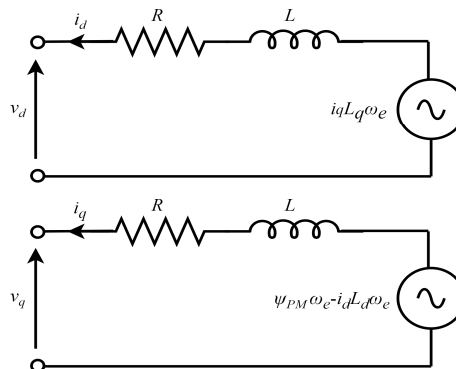

Fig. 9. *d* and *q* axes equivalent to the generator circuit.

Rectification is the process of converting alternating current (AC) to direct current (DC) using an electrical device called a rectifier. In high power applications, one of the most crucial circuits is the three-phase full-wave bridge rectifier. The three-phase source can be directly linked to the rectifier. The rectifier's typical output voltage is [30]:

$$V_r = \left(\frac{3\sqrt{2}}{\pi} \right) V_{LL} \tag{25}$$

where:

V_r : is the DC or average output voltage (V).

V_{LL} : is the AC line voltage (V).

The rectifier's output voltage ripples are eliminated by a filter capacitor using:

$$C_1 = \frac{1}{f_f R R_f} \tag{26}$$

Control strategies play a pivotal role in the effective operation of marine renewable energy conversion systems. These systems, designed to harness the power of the ocean's renewable resources, involve complex physical energy conversion chains. Control strategies are essential for optimizing energy extraction and ensuring the system's robust and efficient performance. In the context of marine renewable energy, control strategies serve several critical functions [31]. Firstly, they help adapt the system to the dynamic and often unpredictable nature of marine conditions, including variations in wave height, frequency, and tidal currents. By continuously monitoring these environmental parameters and adjusting the system's operation, control strategies can maximize energy capture while maintaining the structural integrity of the equipment.

7. Advanced Control Algorithms for Enhanced MPA Performance

Advanced control algorithms that handle many elements of point absorber wave energy converters' functioning, such as DC voltage stabilization and active/reactive power regulation, are necessary to improve their performance. A thorough control system for point absorber wave energy converters should incorporate these control strategies. The particulars of the point absorber system, the environment, and the grid needs will determine the choice of algorithm and controller architecture. For effective control and performance improvement, real-time monitoring and feedback are also essential.

The converter in Fig. 10 is also contrasted with this kind of set up. The benefits of adding an additional DC/DC converter include [32]:

1) Maintains proper inverter-side DC voltage.
2) Modifies switching ratio to control generator-side Power-voltage.
3) Enables switching for selective harmonic elimination (SHE), which reduces losses.
4) The inverter no longer requires control of DC voltage and has more flexible power.

By adjusting the basic line current's specific magnitude and the phase angle between the line current and the line voltage, the inverter can be controlled.

The controller can be configured to switch the VSI at the absolute frequency of the three-sided carrier signal with well-defined output harmonics. For each shaft speed, it is feasible to determine the best electric voltage values that correspond to the highest achievable turbine power. In addition to the DC/AC voltage percentage and power, control variables that can be set to manage the power are used when necessary. The continuity of the DC-link can be preserved by turning the inverter handle, and the active power can be changed to maximize real power transmission. Results show that thyristor-based inverters with active compensators are best suited for powerful HVAC systems since they depend on the device to ensure replacement. However, it is possible to merge the two VSI and Direct current/DC-VSI devices with comparable AC systems. Numerous additional control techniques have also been applied to this convertor [33].

The specific DC/AC inverter is able to control both the active and reactive power provided to the grid by adjusting the q-axis in addition to the already present d-axis. The q-axis reference point current is computed using the inaccuracy inside the DC-link voltage and compared to the current. In order to determine the utility's phase angle, which is used for power factor command, phase locked loop (PLL) technology is used in a d-q synchronous reference frame. Power factor control uses the reference current along the d-axis of the rotation to enable comparisons. The inaccuracy in both coordinate system currents is used to generate the d-q-axis voltages required for space vector PWM control [34].
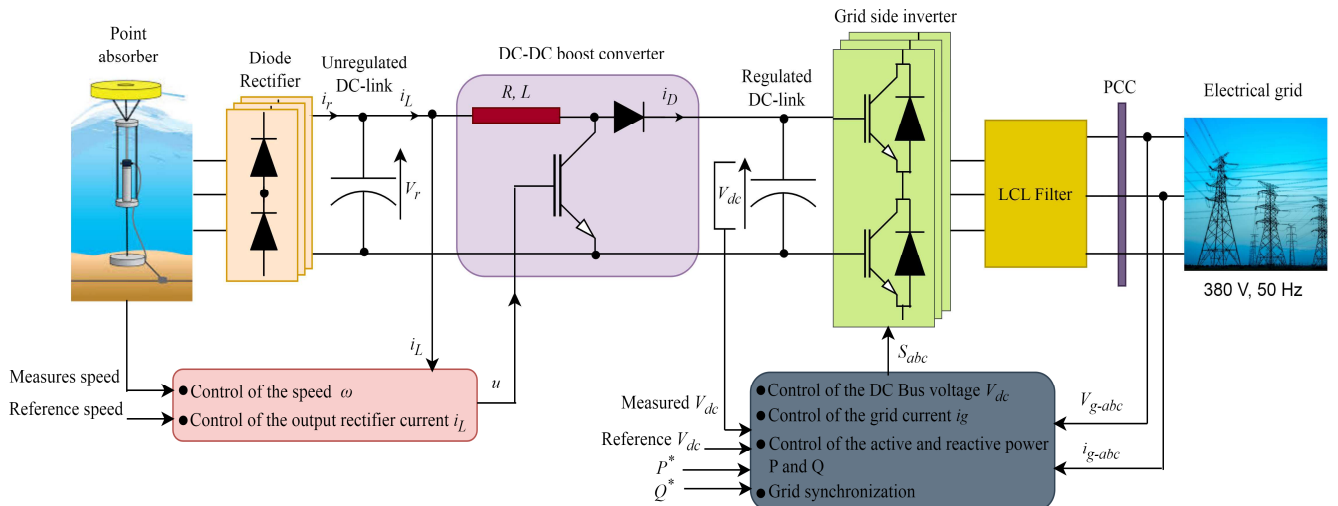

Fig. 10. LPMSG-based wave energy system along with its controller.

With the aid of a boost-controlled DC/DC chopper, a voltage equation control, and a proportional integral (PI) control, the duty ratio of the chopper switch may be computed for any kind of particular optimal position. The benefit of flexible active and reactive power transfer to a particular grid is that the inverter-side DC-link voltage stays constant because it is determined by the actual grid voltage. The ability to tune the chopper output to the maximum value and provide output power is one advantage of the continuous DC-link voltage. The control is implemented by a human relationship between the duty cycle and output power of this chopper [35]. The obligation cycle might begin at any point and go gradually, switching between different ranges in an effort to obtain the largest power distribution point. It is discovered that the system started to lose efficiency at high speeds, this was caused by the duty ratio and DC current's phase i_{ag}.

7.1. Control system of PMSG side converter

The role of the ac-dc converter is to operate the wind turbine at maximum power extraction. This task is performed by adjusting the electrical torque of the machine to operate on the optimal torque curve. In the case of the LPMSG, the control strategy is to regulate the ac current. The diode rectifier does not fulfill this role since this topology provides control over neither the ac current, i_t, nor the output dc current i_r. However, it has been discussed that the dc-dc converter can be used to control the rectifier current i_r. Furthermore, Equation of the DC link has stated the correspondence between the dc current and the ac current [36]. Therefore, the current i_r is the signal regulated using the duty cycle of the dc-dc converter as shown in Fig. 12.

The control approach based constant stator voltage is directly managing the generator stator voltage can be employed to prevent overvoltage of the converter brought on by overspeed of the generator. The control goal is accomplished at the stator voltage reference frame (SVRF), where the vector direction of the stator voltage is assumed to be in the direction of the d-axis. Since the d- and q-axis components of the stator current determine the active power and reactive power, respectively, there is no coupling in this situation [37].

Voltages and currents from the stator of the generator are converted into active P_s and reactive power Q_s by means of Eq. (27). This equation is also identical for both induction machines and permanent magnet machines:

$$\begin{cases} P_s = \dfrac{3}{2} v_{sd} i_{sd} \\ Q_s = -\dfrac{3}{2} v_{sd} i_{sq} \end{cases} \tag{27}$$

The d-axis component of the stator current determines the generator's active power. Through control of the q-axis component, the stator voltage may be maintained at the rated value. A constant stator voltage control technique has the advantage of allowing the converter and generator to continue working at their rated voltages while maintaining a constant V_{dc}/v_{ac} ratio, which prevents over-voltage and converter saturation at high speeds. The converter's rated capacity is raised by the control mode [38].

The best of the three control systems has been found to be constant stator voltage control. In order to maintain the stator voltage of the PMSG at the rated value and the active power at the reference value, or to achieve MPPT of the WEC, the stator current vector control with stator voltage orientation can decouple the active and reactive power of a PMSG.

The stator voltage vector will point in the synchronously spinning reference frame's d-axis direction if the q-axis is rotated 90 degrees counterclockwise along the d-axis direction, giving $v_{sd} = v_s$ and $v_{sq} = 0$. The d- and q-axes are thought to have the same inductive reactance since the LPMSG rotor is symmetrical: $L_d = L_q = L$. The stator voltage and flux linkage equations for the PMSG can be shortened to the following under this supposition:

$$\begin{cases} v_{sd} = R_s i_{sd} + \dfrac{d\psi_{sd}}{dt} - \omega_e \psi_q = v_s \\ v_{sq} = R_s i_{sq} + \dfrac{d\psi_{sq}}{dt} + \omega_e \psi_d = 0 \end{cases} \tag{28}$$

$$\begin{cases} \psi_{sd} = L i_{sd} + \psi_{PM} = 0 \\ \psi_{sq} = L i_{sq} = -\dfrac{v_s}{\omega_s} \end{cases} \tag{29}$$
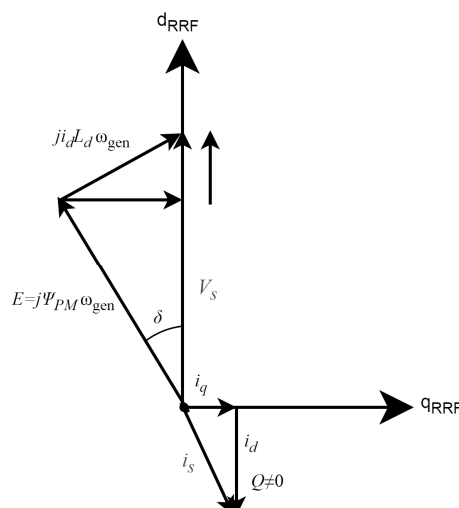

Fig. 11. Vector chart for a constant stator volt generator-side converter control strategy.

Equations (28) and (29) show:

$$\begin{cases} v_{sd} = R_s i_{sd} + L\dfrac{di_{sd}}{dt} - \omega_e L i_{sq} \\[2mm] v_{sq} = R_s i_{sq} + L\dfrac{di_{sq}}{dt} + \omega_e \left(L i_{sd} + \psi_{PM}\right) \end{cases} \tag{30}$$

The LPMSG's combined active and reactive power can be expressed as follows:

$$\begin{cases} P_s = \dfrac{3}{2} v_s i_{sd} \\[2mm] Q_s = -\dfrac{3}{2} v_s i_{sq} \end{cases} \tag{31}$$

As a result, the SVRF entirely decouples the active and reactive currents, while coupling the associated control voltage vectors. The following two new inputs can be defined:

$$\begin{cases} v'_{sd} = v_{sd} + \omega_e L i_{sq} \\[2mm] v'_{sq} = v_{sq} - \omega_e L i_{sd} \end{cases} \tag{32}$$

If we substitute (32), we obtain:

$$\begin{cases} v'_{sd} = R_s i_{sd} + L\dfrac{di_{sd}}{dt} \\[2mm] v'_{sq} = R_s i_{sq} + L\dfrac{di_{sq}}{dt} + \omega_e \psi_{PM} \end{cases} \tag{33}$$

As a result, feedforward compensation can be used to create decoupled control of current by adding feedforward inputs ($\omega_e L i_{sq}$ and $\omega_e L i_{sd}$) to the d- and q-axes current controllers.

The relationship between the AC and DC voltages for the PWM converter can be represented as follows:

$$\begin{cases} v_{sd} = \dfrac{\sqrt{3}}{2\sqrt{2}} P_{md} V_{dc} \\[2mm] v_{sq} = \dfrac{\sqrt{3}}{2\sqrt{2}} P_{mq} V_{dc} \end{cases} \tag{34}$$

The generator side converter's power circuit and speed control are shown in Fig. 12. Take note that Maximum Power Point Tracking (MPPT) techniques are typically used to calculate the electric rotational speed reference. These methods try to modify the PMSG rotor speed (by modifying its reference) in order to maximize power extraction for a specific wind speed value. In this paper, the MPPT control is not taken into account [39, 40].

A synchronization grid technique is needed in order to provide synchronized values for the inverted voltage's amplitude, phase, and frequency—values that are considered variables and crucial pieces of information for the grid-connected inverter systems. The synchronization approach links the grid voltage and the magnitude and angle of the VSI reference currents [41]. This equipment and its functioning require quick and precise detection of the amplitude, phase angle, and frequency of the VSI's inverted voltage in order to assure proper creation of reference signals and comply with grid connected system rules. Grid-connected WEC have been managed to function as closely as feasible to the unity power factor, though, in order to meet minimum power dissipation requirements and comply with grid code restrictions [42]. Phase Locked Loop (PLL) and Filtered Zero Cross Detection (ZCD) are two crucial synchronization techniques that can be employed for this [43].
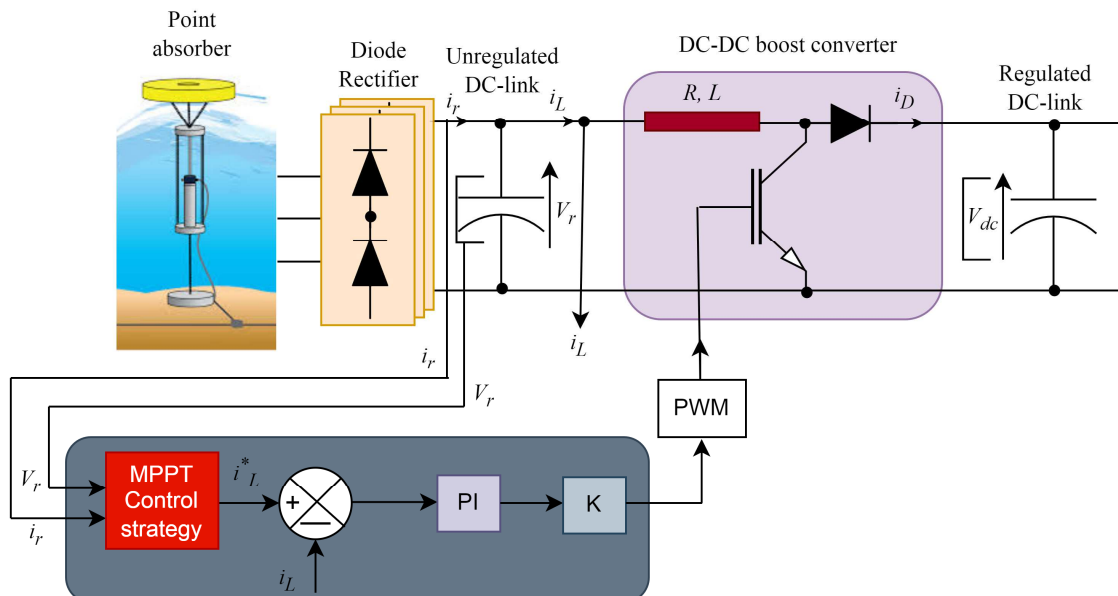

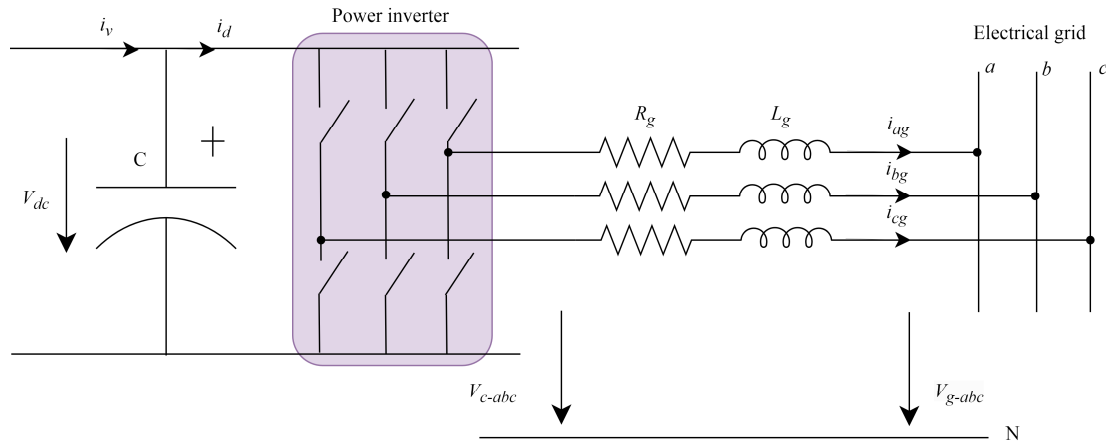Fig. 12. Power circuit of the generator side converter along with its speed control.

Fig. 13. Diagram of the PWM voltage source converter at the grid.

7.2. Grid-side converter control system

To accomplish decoupled control of the active and reactive power between the grid and the grid-side converter, voltage-oriented vector control is used to control the grid-side converter. It is largely utilized to control the reactive power between the WEC and the grid as well as the DC voltage of the DC link. Its control goals are as follows [44]:

- Maintain a steady DC voltage
- Maintain the reference value for the reactive power exchanged between the grid and the grid-side converter.

Figure 13 displays the structure diagram of the grid-side PWM voltage source converter. Figure 13 displays:

$$\begin{bmatrix} V_{ga} \\ V_{gb} \\ V_{gc} \end{bmatrix} = R_g \begin{bmatrix} i_{ga} \\ i_{gb} \\ i_{gc} \end{bmatrix} + L_g \frac{d}{dt} \begin{bmatrix} i_{ga} \\ i_{gb} \\ i_{gc} \end{bmatrix} + \begin{bmatrix} V_{ca} \\ V_{cb} \\ V_{cc} \end{bmatrix} \tag{35}$$

where:

V_{gabc} : is the three-phase grid voltage (V),
V_{cabc} : is the three-phase grid-side converter voltage (V),
i_{ga}, i_{gb}, i_{gc} : are the three-phase grid-side converter currents (A),
R_g and L_g : are series resistance (Ω) and inductance (H) of the grid-side converter,
i_d and i_v : are the DC currents (A) of the grid-side and the generator, and C is the DC-link capacitance.

We may obtain the voltage equation in the *dq* synchronously rotating frame using a PARK transformation of (33):

$$\begin{cases} V_{gd} = R_g i_{gd} + L_g \dfrac{di_{gd}}{dt} - \omega_0 L_g i_{gq} + V_{cd} \\ V_{gq} = R_g i_{gq} + L_g \dfrac{di_{gq}}{dt} + \omega_0 L_g i_d + V_{cq} \end{cases} \tag{36}$$

where i_{gd}, i_{gq}, v_{gd}, and v_{gq}: are the *d* and *q*-axis components of the grid current and voltage, and V_{cd} and V_{cq} are the *d*- and *q*-axis components of the converter voltage at the grid-side.

The grid-side converter and the grid can exchange active power P_g and reactive power Q_g as follows:

$$\begin{cases} P_g = \dfrac{3}{2}\left(V_{gd}i_{gd} + V_{gq}i_{gq}\right) \\ Q_g = \dfrac{3}{2}\left(V_{gq}i_{gd} - V_{gd}i_{gq}\right) \end{cases} \tag{37}$$

In this part, grid-voltage-oriented vector control is used, with the q-axis rotating 90 degrees along the d shaft and the grid-voltage direction being the direction of the d-axis. In this instance, the grid-voltage vector's q-axis component, V_{gq}, equals 0, and:

$$\begin{cases} P_g = \dfrac{3}{2}V_{gd}i_{gd} \\ Q_g = -\dfrac{3}{2}V_{gd}i_{gq} \end{cases} \tag{38}$$

V_{gd} is constant if the grid voltage is assumed to be constant. Then, i_{gd} and i_{gq}, respectively, govern the active power P_g and reactive power Q_g exchanged between the grid and the grid-side converter [45].

Switching loss, a significant converter loss, can be compared to a resistor placed between the DC link's poles. Both the loss and the loss in the converter's series resistor can be disregarded because of how little the loss is. If we assume that the converter is an ideal converter, we may get the equation shown below:

$$V_{dc}i_{dc} + \sqrt{3}\,\mathrm{Re}\left(\dot{V}_{dc}i_{dc}^*\right) = 0 \tag{39}$$

With those words:

$$V_{dc}i_{dc} = \sqrt{3}V_{gd}i_{gd} = P_g \tag{40}$$

The PWM converter's relationship between the AC and DC voltages is rewritten as follows:

$$\begin{cases} V_{gd} = \dfrac{\sqrt{3}}{2\sqrt{2}} P_{md} V_{dc} \\ V'_{gq} = \dfrac{\sqrt{3}}{2\sqrt{2}} P_{mq} V_{dc} \end{cases} \tag{41}$$

where P_{md} and P_{mq} are the grid-side converter's PWM modulation factors:

$$i_d = \frac{3}{2\sqrt{2}} P_{md} i_{cd} \tag{42}$$

The formula below is accurate for capacitor C in the DC loop:

$$C\frac{dV_{dc}}{dt} = i_d - i_v \tag{43}$$

The following is how the DC voltage V_{dc} and the active component of the grid current, i_{gd}, are related:

$$C\frac{dV_{dc}}{dt} = \frac{3}{2\sqrt{2}} P_{md} i_{gd} - i_v \tag{44}$$

We can obtain the transfer function with the DC voltage V_{dc} as the output and the grid current active component i_{gd} as the input by performing a Laplace transformation of the aforementioned equation with I acting as a disturbance variable:

$$\frac{V_{dc}(s)}{i_{gd}(s)} = \frac{3P_{md}}{2\sqrt{2}Cs} \tag{45}$$

Equation 45 demonstrates that i_{gd} regulates the DC-link voltage V_{dc}. The relationship between the inverter voltage (V_{cabc}) and the current (i_{gd}/i_{gq}) must be established because the converter is ultimately controlled by the voltage. In equation (34), we presumptively believe [46]:

$$\begin{cases} V'_{gd} = R_g i_{gd} + L_g \dfrac{di_{gd}}{dt} \\ V'_{gq} = R_g i_{gq} + L_g \dfrac{di_{gq}}{dt} \end{cases} \tag{46}$$

Equation (36), when changed, becomes:

$$\begin{cases} V_{cd} = V_{gd} - V'_{gd} + \omega_e L_g i_{gq} \\ V_{cq} = -V'_{gq} - \omega_e L_g i_{gd} \end{cases} \tag{47}$$

The transfer function with grid current i_g as the output and V'_g as the input can be obtained using the Laplace transform of (45):

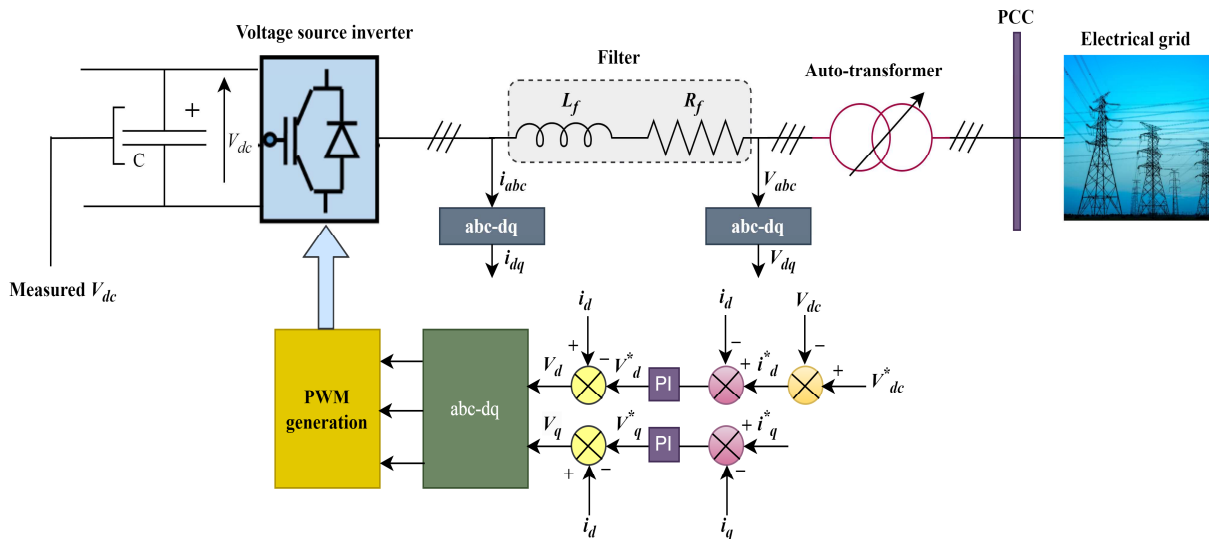$$\frac{i_{gd}(s)}{V'_{gd}(s)} = \frac{i_{gq}(s)}{V'_{gq}(s)} = \frac{1}{L_g s + r_g} \tag{48}$$

Fig. 14. Grid side inverter control and DC voltage stabilization.

Table 1. LPMSG parameters.

Rotor flux linkage magnitude (Wb)	Stator Resistance (Ω)	Auto-inductance of the d axis (H)	Auto-inductance of the d axis (H)	Pair poles	Viscous friction Coefficient (kg.s⁻¹)	Moment of inertia (kg.m²)
1.429	0.008	0.454	0.454	18	0.0028	0.002008

Table 2. Boost converter parameters.

Inductor internal Resistor (Ω)	Inductor internal Inductance (H)	Uncontrolled Capacitor (μF)
0.1	0.007	1000

Table 3. Electric filter and grid parameters.

Resistance of the filter (Ω)	Inductance of the filter (H)	Grid voltage (V)	Frequency (Hz)	DC capacitor (mF)	DC link voltage (V)
10	0.5	380	50	10	1000

In this paper, we delve into the realm of renewable energy with a focus on advanced control strategies for multi-point absorbers. The abstract asserts the effectiveness of these innovative control approaches, substantiated through a meticulous combination of simulations and real-world experiments. The evaluation criteria encompass critical aspects such as energy conversion efficiency, grid compatibility, and system reliability, underlining a comprehensive assessment of the proposed strategies. By subjecting the advanced control strategies to diverse conditions, the study aims to showcase their adaptability and superiority compared to conventional methods. This research not only promises advancements in the field of wave energy conversion but also contributes valuable insights that bridge the gap between theoretical concepts and practical implementation, offering a promising pathway for sustainable and reliable power generation.

8. Simulation Validation and Performance Evaluation

The modeling results of a point absorber WEC based on a 200 kW LPMSG technology are shown in this section. Figure 5 depicts the LPMSG-based WEC system that was modelled in the Matlab/Simulink environment. In Tables 1, 2 and 3, respectively, we also offer the LPMSG, boost converter parameters and the electric filter and grid connection parameters. Under stochastic wave speed fluctuations, the efficiency and viability of applying the advanced control to the side generator and grid via a boost converter and the voltage source inverter architecture are explored.

The switching frequency of the grid-side inverter is specified to be the same as that of the inverter controlling the LPMSG since it is assumed that the two inverters under discussion are perfect. Selections have been made for the filter resistance, inductance, capacitor capacity, and DC link voltage.

Three objectives are intended to be achieved by the simulation of the multi-point absorber model with grid connection: first, to examine the behavior of significant system variables over time; second, to confirm that power generated by the PTO is successfully injected into the grid; and third, and to confirm that current is injected into the grid with unity power factor. A simulation time of 30 seconds was found adequate to accomplish these goals. The applied wave form with an amplitude of 1 m, the rod speed, the position of the buoy, the force produced is 250 kN and the response of the point absorber are just a few of the variables that are shown in Fig. 14 as trends over time.
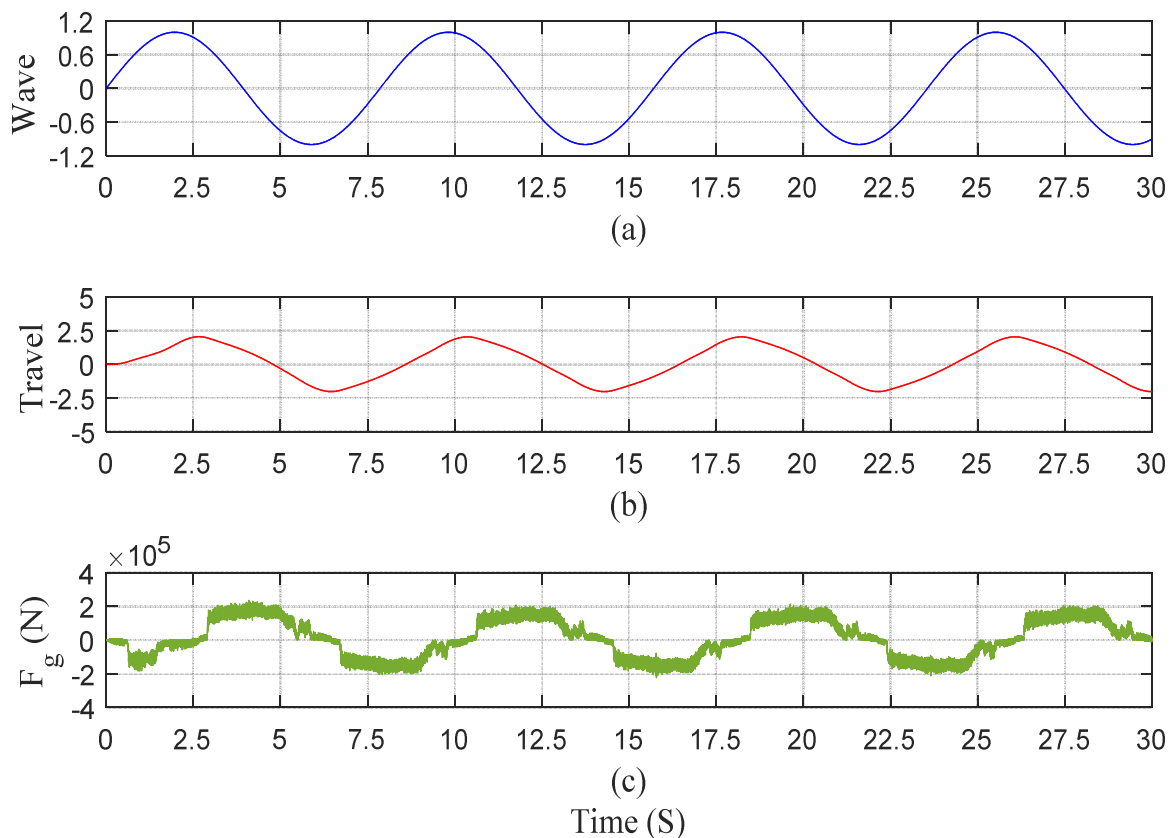

Fig. 15. Time evolution of key variables in the WEC based multi-point absorber model, (a) wave signal, (b) travel curve, (c) force curve.
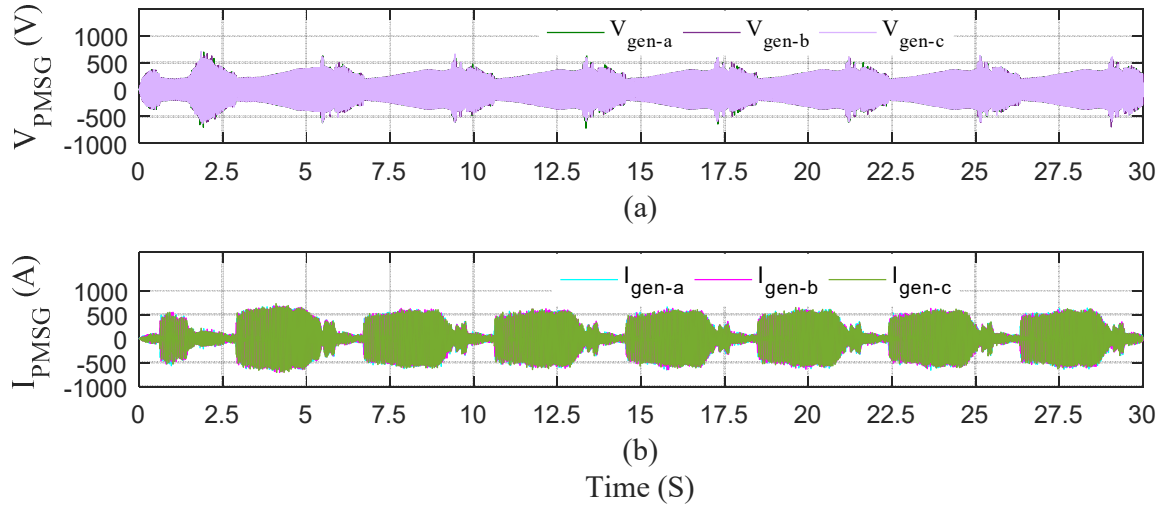
Fig. 16. Three-phase voltage and current output from the generator respectively during typical sea operation.
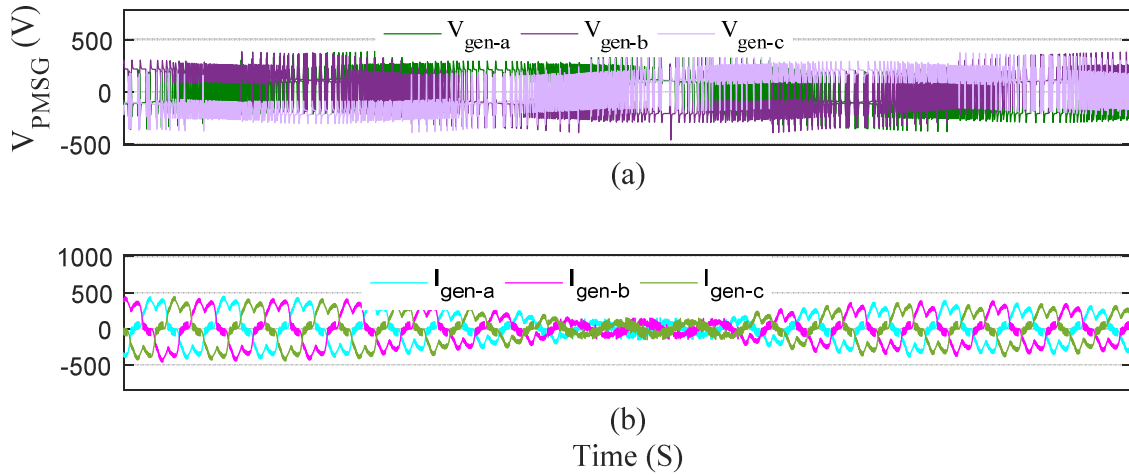

Fig. 17. Zoom of electrical variables of the PSMG: (a) voltage of the generator, (b) current of the generator.

Figure 15 shows the simulation responses that were produced in order to evaluate the transient and steady state performances of the investigated predictive controllers under sudden changes in wave speed. According to Fig. 18 (a), which shows the LPMSG rotational velocity response to wave speed under the predictive model controllers, both regulators operate well in steady state. Figure 18 (b) shows the electromagnetic torque that the generator generated.

As a result, it can be inferred that the DC voltage regulation depicted in Fig. 20 (a) is functioning properly and that the power produced by the PTO is directly injected into the grid due to the nearly constant DC link voltage of the capacitor. A constant DC connection voltage suggests that the capacitor will gradually store energy steadily over time.

The diode's inherent commutation is what results of the distortion in Figs. 16 (a) and (b) of the stator voltage and current waveforms of the LPMSG. Despite being zoomed in on in Figs. 17 (a) and (b), the fundamental stator voltage and current components are in phase, demonstrating the achievement of unity power factor functioning. Harmonics produced by the three-phase currents of the LPMSG cause waves in the electromagnetic torque (T_{em}) which reaches a maximum value of 250.10^3 N.m as shown in Fig. 18 (b). The grid-side inverter adjusts the net dc-bus voltage and reactive power to their respective reference values while the control strategy guarantees that the dc-link current i_{dc} is kept at its reference value.

Grid voltage and current are shown in figures 20 (b) and (c), respectively, along with their enlarged perspectives in Fig. 21 (a) and (b). These demonstrate that the OWC's unity power factor is accurate. These findings demonstrate the electronic power inverter's effective regulation, which is supported by the continuous upkeep of the DC bus voltage. It is evident that the oscillations in the generator's speed are associated with the variations in the grid current and DC link voltage waveforms.

The tracing performance of the converter output is shown in Figs. 19 (a), (b), and (c). It should be noted that oscillations exist in the current, voltage, and power produced by the rectifier, which need to be filtered and controlled before being injected into the electrical network by the voltage inverter. After performing current and voltage filtering, the step-up chopper ensures control of these variables. In order to achieve exceptionally high active energy yields and extremely stable direct bus voltages, the suggested control technique necessitates that the reactive energy have a value of zero during the simulation period, as shown in Fig. 20 (d).

Figure 18 (c) shows the active and reactive power components of the generator; the control law applied shows a decent decoupling of the two components. According to Fig. 20 (d), the suggested control technique compels the reactive energy to have a value of zero during the simulation period, allowing for a very high active energy yield and a very steady direct bus voltage. The input power and grid power values stabilize at a new steady-state value once the LPMSG speed reaches the new reference value. However, the voltage source inverter management technique successfully balances the DC-link capacitor voltages even though the net DC-bus voltage deviates from its reference value during this time.
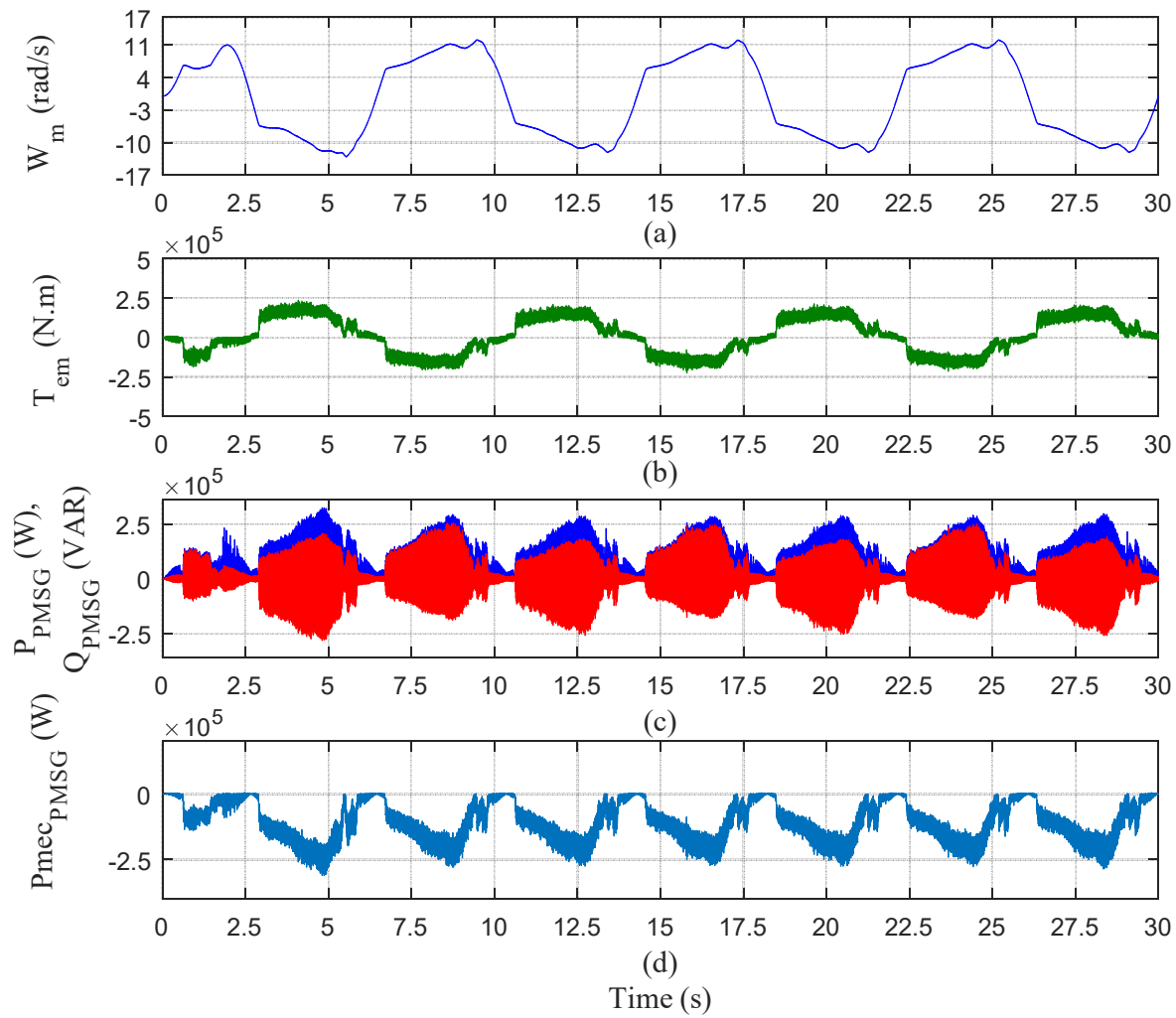
Fig. 18. Mechanical and electrical variables of the PSMG during the testing of marine substation: (a) speed of the generator, (b) electromagnetic torque developed by the generator, (c) electrical power, (d) mechanical power.
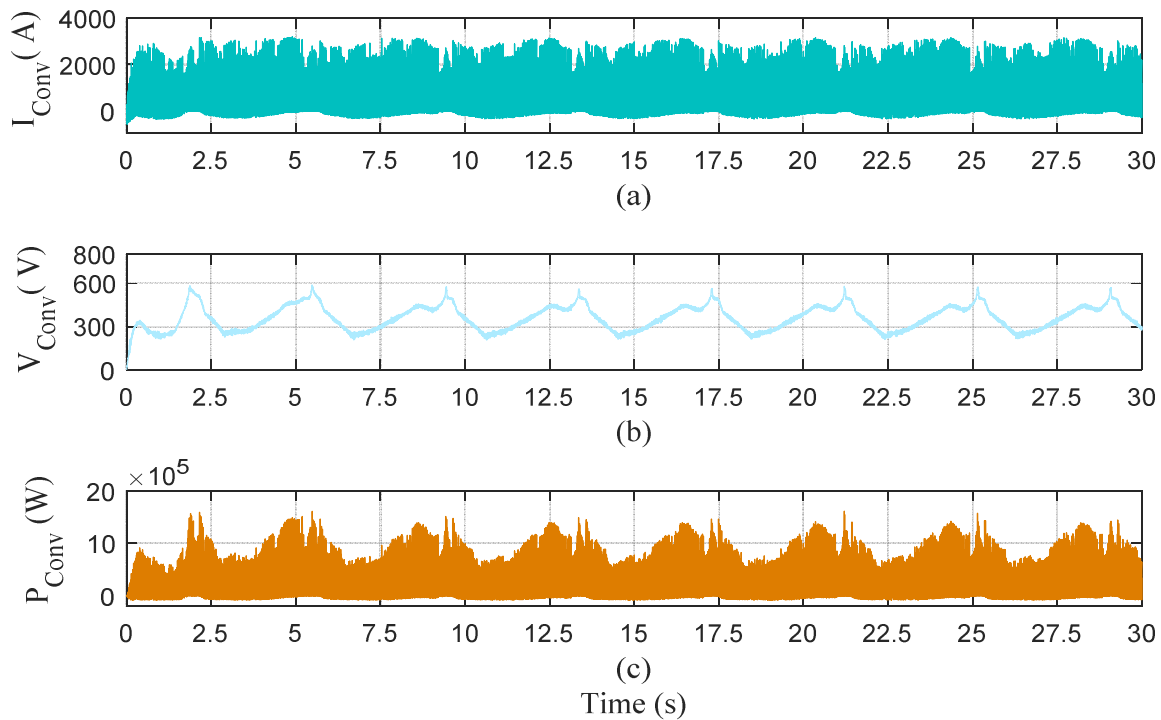

Fig. 19. The tracking performance of the converter output, (a) output current, (b) output voltage, (c) output power.
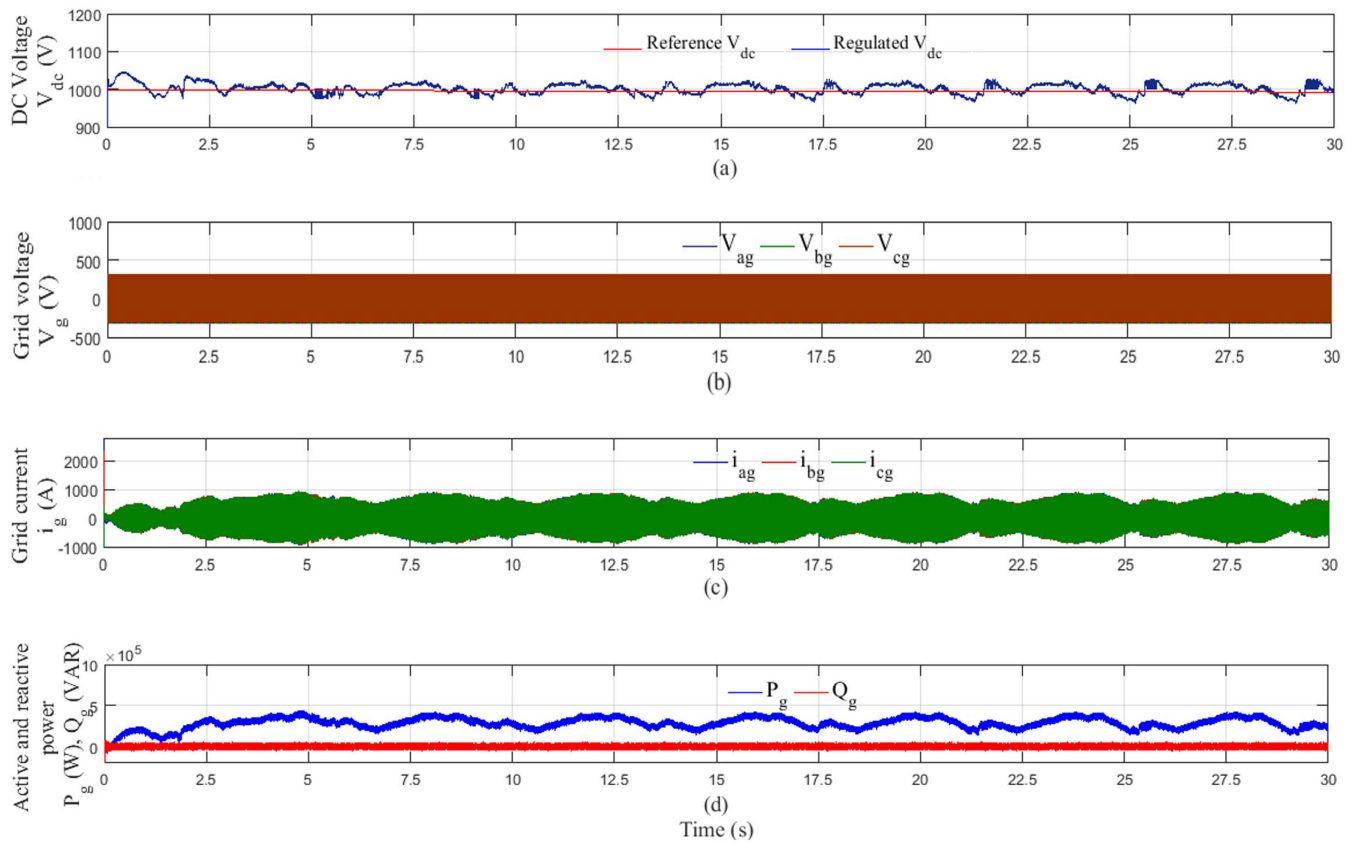
Fig. 20. Performance of the grid connection system: (a) Regulated DC link voltage under wave fluctuation, (b) Three phase grid voltages, (c) Three phase injected grid currents, (d) Active and reactive power injected into the grid.
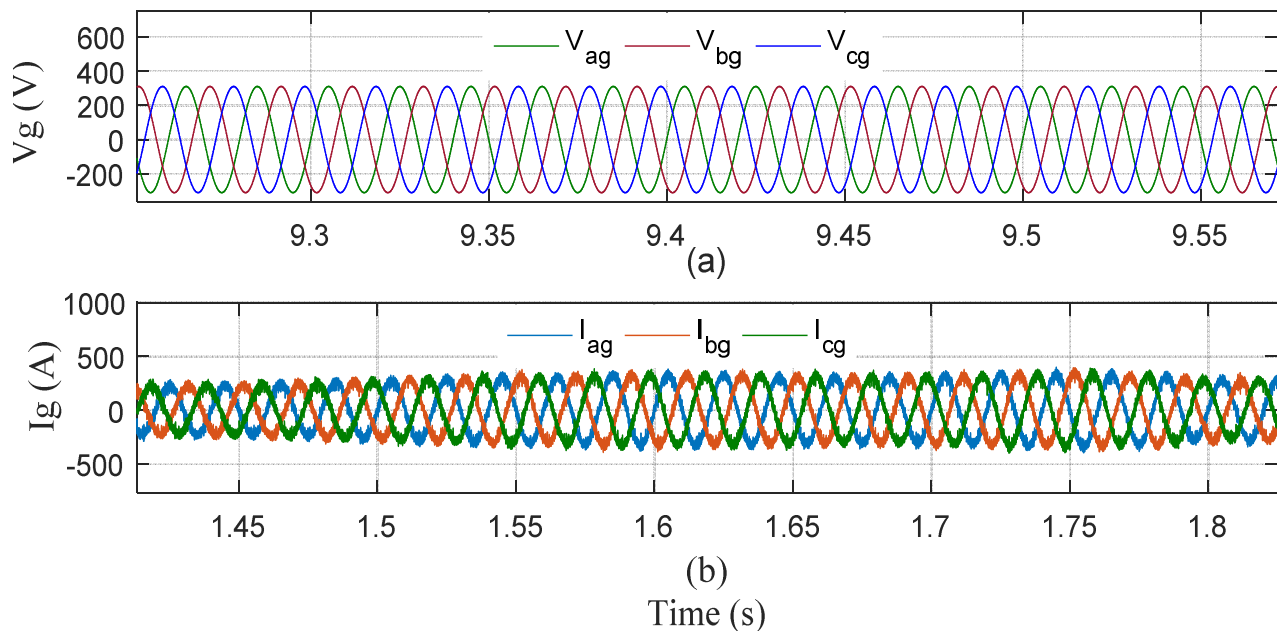
Fig. 21. (a) Zoom of three phase grid voltages, (b) Zoom of three phase injected grid current.

The speed, electromagnetic torque developed and mechanical power of the generator are shown in Figs. 18 (a), (b) and (d) respectively. The quantities generated by numerical simulation show that the appearance of the mechanical and electrical quantities have the same behavior of the appearance of the applied wave, the power generated is 250 kW, the analysis of these curves shows the reflection of the nature of the energy produced and its environment which has an influence and a direct impact of the primary energy on the energy produced.

Signal
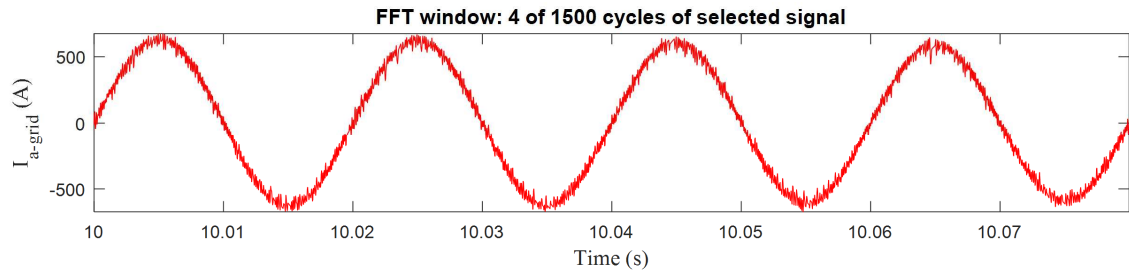
FFT analysis
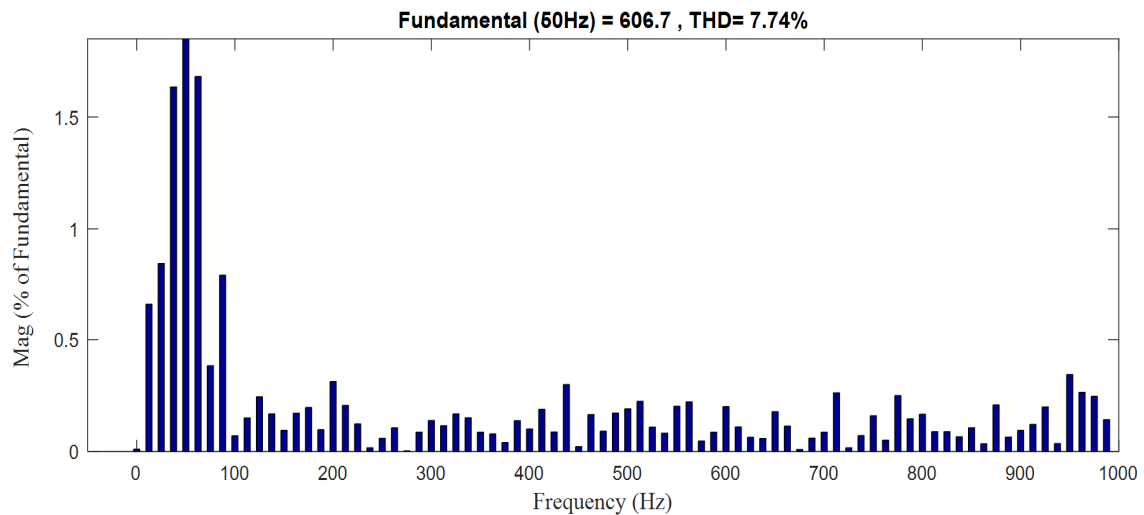
Fig. 22. Spectral analysis of the current i_{ag} in grid side.

The generator active and reactive power components are illustrated in Fig. 18 (c), there is a good decoupling of the two components according to the control law applied. From Fig. 20 (d), the proposed control technique forces the active energy to have a zero value during the simulation period, which makes it possible to have a very high active energy yield and this setting also makes it possible to have a direct bus voltage very stable. Once the LPMSG speed reaches the new reference value, the input power and the grid power values stabilize at a new steady-state value. Although the net DC-bus voltage deviates from its reference value during this period, the voltage source inverter control strategy effectively balances the DC-link capacitor voltages. Figure 20 (a) and (d) shows the active power grid waveform and DC link voltage waveform when the applied wave oscillates. The DC bus voltage oscillates around an amplitude value of 1000 V. Fluctuations of approximately 1.5 % of the nominal value appear on this voltage which corresponds to a variation in the waveform of the applied wave. The grid current of 200 A and the zero-phase angle between the grid voltage and current due to the zero reactive power reference are shown in figure 20 (c) with the zoom on figure 21 (b). Amounts of 400 kW and 0 VAR, respectively, are listed as the apparent active and reactive power. To confirm the power quality, Figure 22 displays a comprehensive plot of the phase a current at the grid sector. The red line represents the current waveform. It is clear that both waveforms are sinusoidal, indicating that the targeted current injection into the grid was successful and resulted in good power quality. It is important to note that during this operation, the generator's rated output is lower than the mechanical input power. In the same figure, we observe the value of the THD of the current injected into the network is 7.74 % which is close to the international standard.

It is feasible to identify any flaws or challenges with the suggested control system, as well as areas for improvement, through examination of the simulation data. The results show that the analyzed system has good stability and very low noise and vibration levels, which may be an indication of how well the recommended system design and control strategy work. The acquired simulation findings and in-depth talks are crucial for assessing the viability and potential of predictive control for a MPA-LPMSG systems and can direct future study and advancement in this field.

9. Conclusion

In the quest for a sustainable and renewable energy future, this study delves into advanced control strategies tailored for Multi-Point Absorber (MPA) systems, focusing on performance enhancement and seamless grid integration within both AC and DC networks. The exploration uncovers a myriad of opportunities and innovations that hold the potential to transform wave and tidal energy into a reliable power source. Our examination of MPA technologies reveals unique challenges and potentials, prompting the development of adaptive control algorithms capable of real-time adjustments to dynamic marine environments. These strategies, rooted in wave and tidal patterns, optimize energy extraction while preserving MPA structural integrity, significantly enhancing energy conversion efficiency. The study emphasizes the transformative impact of advanced controls on unlocking the true potential of MPA systems.

Addressing the challenge of grid integration, we recognize the global diversity of electrical grid and explore innovative power electronics interfaces and synchronization techniques. These innovations bridge the gap between MPA systems and AC/DC grids, ensuring their effective and reliable contribution to grid stability. The bidirectional power flow capabilities of MPAs further enhance grid support functions, reinforcing their adaptability in the evolving energy landscape. Empirical validation of advanced control strategies through extensive simulation studies yields unequivocal evidence of their effectiveness and robustness. This study concerns the integration of a medium power MPA power plant of 250 kW, integrated into a 400 V, 50 Hz network with 1000 V

intermediate circuit. The demonstrated improvements in energy conversion efficiency, grid integration compatibility, and system reliability under various conditions underscore the potential of these strategies to revolutionize the renewable energy sector.

This paper outlines a holistic framework for developing and deploying advanced control systems tailored explicitly to Multi-Point Absorber technology. By addressing challenges and capitalizing on opportunities, we take a significant step towards achieving efficient and sustainable wave and tidal energy utilization. As the world strives for cleaner energy sources, the innovations unveiled here present a compelling path forward, contributing tangibly to a greener and more resilient global energy landscape. Further development, testing, and validation of the instantaneous hydrodynamics force computation capability outlined in this research will be the focus of our future work on this area. We also intend to use WEC-Simulator to investigate the effects of adding instantaneous force calculations on the annual average power production of wave energy devices predicted by numerical simulations.

Author Contributions

A. Alnujaie and A. Berkani planned the scheme, initiated the project, and suggested the simulation; K. Negadi and L. Hadji conducted the simulation and analyzed the empirical results; M.H. Ghazwani developed the mathematical modeling and examined the theory validation. The manuscript was written through the contribution of all authors. All authors discussed the results, reviewed, and approved the final version of the manuscript.

Acknowledgments

Conflict of Interest

The authors declared no potential conflicts of interest concerning the research, authorship, and publication of this article.

Funding

Data Availability Statements

The datasets generated and/or analyzed during the current study are available from the corresponding author on reasonable request.

Nomenclature

AC	Alternative current	PI	Proportional integral
DC	Direct current	NWTs	Numerical wave tanks
PTO	Power take-off	ZCD	Zero Cross Detection
LPMSG	Linear permanent magnet synchronous generator	HVAC	High voltage alternative current
VSI	Voltage source inverter	PWM	Pulse width modulation
MPA	Multi-point absorber	MPPT	Maximum power point tracking
PLL	Phase locked loop	SVRF	Stator voltage reference frame
NPC	Neutral Point Clamped	WEC	Wave energy converter
SHE	Selective harmonic elimination		

References

[1] Shi, H., Cao, F., Liu, Z., Qu, N., Theoretical study on the power take-off estimation of heaving buoy wave energy converter, *Renewable Energy*, 86, 2016, 441–448.

[2] Beatty, S.J., Bocking, B., Bubbar, K., Buckham, B.J., Wild, P., Experimental and numerical comparisons of self-reacting point absorber wave energy converters in irregular waves, *Ocean Engineering*, 173, 2019, 716–731.

[3] Beatty, S.J., Hall, M., Buckham, B.J., Wild, P., Bocking, B., Experimental and numerical comparisons of self-reacting point absorber wave energy converters in regular waves, *Ocean Engineering*, 104, 2015, 370–386.

[4] Zhao, A., Wu, W., Sun, Z., Zhu, L., Lu, K., Chung, H., Blaabjerg, F., A Flower Pollination Method Based Global Maximum Power Point Tracking Strategy for Point-Absorbing Type Wave Energy Converters, *Energies*, 12(7), 2019, 1343.

[5] Artal-Sevil, J.S., Domínguez, J.A., El-Shalakany, H., Dufo, R., Modeling and simulation of a wave energy converter system. Case study: Point absorber, *Thirteenth International Conference on Ecological Vehicles and Renewable Energies (EVER)*, Monte Carlo, Monaco, 2018.

[6] Hai, L., Svensson, O., Isberg, J., Leijon, M., Modelling a point absorbing wave energy converter by the equivalent electric circuit theory: A feasibility study, *Journal of Applied Physics*, 117, 2015, 164901.

[7] Blaabjerg, F., Yang, Y., Ma, K., Wang, X., Advanced Grid Integration of Renewables Enabled by Power Electronics Technology, *Nachhaltige Energieversorgung und Integration von Speichern: Tagungsband zur NEIS*, Springer Fachmedien Wiesbaden, 2015.

[8] Engin, C.D., Yesildirek, A., Designing and modeling of a point absorber wave energy converter with hydraulic power take-off unit, *4th International Conference on Electric Power and Energy Conversion Systems (EPECS)*, Sharjah, United Arab Emirates, 2015.

[9] Bonaventura, T., Martínez Estévez, I., Domínguez, J.M., Crespo, A.J.C., Göteman, M., Engström, J., Gómez-Gesteira, M., A numerical study of a taut-moored point-absorber wave energy converter with a linear power take-off system under extreme wave conditions, *Applied Energy*, 311, 2022, 118629.

[10] Fekkak, B., Menaa, M., Loukriz, A., Kouzou, A., Control of grid-connected PMSG-based wind turbine system with back-to-back converters topology using a new PIL integration method, *International Transactions On Electrical Energy Systems*, 31(6), 2021, e12882.

[11] Giannini, G., Sandy D., Rosa-Santos, P., Taveira-Pinto, F., A Novel 2-D Point Absorber Numerical Modelling Method, *Inventions*, 6(4), 2021, 75.

[12] Xu, J., Yansong Y., Yantao H., Tao, X., Yong Z., MPPT Control of Hydraulic Power Take-Off for Wave Energy Converter on Artificial Breakwater, *Journal of Marine Science and Engineering*, 8(5), 2020, 304.

[13] Curtis, J.R., *Scaling of Point-Absorber Wave Energy Converter Hydrodynamics*, Doctor of Philosophy, University of Washington, 2021.

[14] Madhana, R., Geetha M., Power enhancement methods of renewable energy resources using multiport DC-DC converter: A technical review, *Sustainable Computing: Informatics and Systems*, 35, 2022, 100689.

[15] Vervaet, T., Stratigaki, V., De Backer, B., Stockman, K., Vantorre, M., Troch, P., Experimental Modelling of Point-Absorber Wave Energy Converter

Arrays: A Comprehensive Review, Identification of Research Gaps and Design of the WECfarm Setup, *Journal of Marine Science and Engineering*, 10, 2022, 1062.

[16] Berkani, A., Negadi, K., Allaoui, T., Marignetti, F., Sliding mode control of wind energy conversion system using dual star synchronous machine and three level converter, *TECNICA ITALIANA-Italian Journal of Engineering Science*, 63(2-4), 2019, 243-250.

[17] Boff, B.H.B., Flores, J.V., Flores Filho, A.F. et al., Dynamic Modeling of Linear Permanent Magnet Synchronous Motors: Determination of Parameters and Numerical Co-simulation, *Journal of Control, Automation and Electrical Systems*, 32, 2021, 1782–1794.

[18] Christian K., Andreas K., Wolfgang K., Modeling of a permanent magnet linear synchronous motor using magnetic equivalent circuits, *Mechatronics*, 76, 2021, 102558.

[19] Sheikh-Ghalavand, B., Vaez-Zadeh, S., Isfahani, A.H., An Improved Magnetic Equivalent Circuit Model for Iron-Core Linear Permanent-Magnet Synchronous Motors, *IEEE Transactions on Magnetics*, 46(1), 2010, 112-120.

[20] Wen-Jun, X., Permanent Magnet Synchronous Motor with Linear QuadraticSpeed Controller, *Energy Procedia*, 14, 2012, 364-369.

[21] Chenyu Z., Feifei C., Hongda S., Optimisation of heaving buoy wave energy converter using a combined numerical model, *Applied Ocean Research*, 102, 2020, 102208.

[22] Yassin, H., Tania Demonte G., Gordon P., David W., Effect of the Dynamic Froude–Krylov Force on Energy Extraction from a Point Absorber Wave Energy Converter with an Hourglass-Shaped Buoy, *Applied Sciences*, 13(7), 2023, 4316.

[23] Sung-Jae, K., Weoncheol, K., Moo-Hyun, K., The effects of geometrical buoy shape with nonlinear Froude-Krylov force on a heaving buoy point absorber, *International Journal of Naval Architecture and Ocean Engineering*, 13, 2021, 86-101.

[24] Vervaet, T., Vasiliki, S., Brecht, D.B., Kurt, S., Marc, V., Peter, T., Experimental Modelling of Point-Absorber Wave Energy Converter Arrays: A Comprehensive Review, Identification of Research Gaps and Design of the WECfarm Setup, *Journal of Marine Science and Engineering*, 10(8), 2022, 1062.

[25] Falnes, J., Kurniawan, A., Fundamental formulae for wave-energy conversion, *Royal Society Open Science*, 2, 2015, 140305.

[26] Dekali, Z., Lotfi B., Thierry, L., Boumediene, A., Grid Side Inverter Control for a Grid Connected Synchronous Generator Based Wind Turbine Experimental Emulator, *European Journal of Electrical Engineering*, 23(1), 2021, 1-7.

[27] Mekhiche, M., Edwards, K., Bretl, J., Ocean Power Technologies PowerBuoy: System-level Design, Development and Validation Methodology, *Proceedings of the 2nd Marine Energy Technology Symposium (METS2014)*, Seattle, WA, 2014.

[28] Araria, R., Negadi, K., Boudiaf, M., Marignetti, F., Non-linear control of dc-dc converters for battery power management in electric vehicle application, *Przeglad Elektrotechniczny*, 1(3), 2020, 84-90.

[29] Zhou, X., Zhou, Y., Ma, Y., Yang, L., Yang, X., Zhang, B., DC Bus Voltage Control of Grid-Side Converter in Permanent Magnet Synchronous Generator Based on Improved Second-Order Linear Active Disturbance Rejection Control, *Energies*, 13, 2020, 4592.

[30] Blanco, M., Moreno-Torres, P., Lafoz, M., Ramírez, D., Design Parameters Analysis of Point Absorber WEC via an evolutionary-algorithm-based Dimensioning Tool, *Energies*, 8, 2015, 11203-11233.

[31] Said, H.A., Ringwood, J.V., Grid integration aspects of wave energy—Overview and perspectives, *IET Renewable Power Generation*, 15, 2021, 3045–3064.

[32] Qiuwei, W., Yuanzhang, S., *Modeling and Modern Control of Wind Power*, Wiley-IEEE Press, 2017.

[33] Noori Khezrabad, A., Rahimi, M., Performance and dynamic response enhancement of PMSG- based wind turbines employing boost converter-diode rectifier as the machine-side converter, *Scientia Iranica*, 29(3), 2022, 1523-1536.

[34] Ibrahim, R.A., Zakzouk, N.E., A PMSG Wind Energy System Featuring Low-Voltage Ride-through via Mode-Shift Control, *Applied Sciences*, 12, 2022, 964.

[35] Toriki, M.B., Asy'ari, M.K., Musyafa', A., Enhanced performance of PMSG in WECS using MPPT – fuzzy sliding mode control, *Journal Européen des Systèmes Automatisés*, 54(1), 2021, 85-96.

[36] Lopez-Flores, D.R., Duran-Gomez, J.L., Vega-Pineda, J., Discrete-Time Adaptive PID Current Controller for Wind Boost Converter, *IEEE Latin America Transactions*, 21(1), 2022, 98–107.

[37] Ahmed E., *Different Control Strategies for PMSG Connected Wind Turbine System*, Computer Science, Aix-Marseile Université, 2022.

[38] Kavousi, A., Fathi, S.H., Milimonfared, J., Soltani, M.N., Application of Boost Converter to Increase the Speed Range of Dual-Stator Winding Induction Generator in Wind Power Systems, *IEEE Transactions on Power Electronics*, 33(11), 2018, 9599-9610.

[39] Gannoun, M., Arbi-Ziani, J., Naouar, M.W., Monmasson, E., Speed Controller design for a PMSG based small wind turbine system, *6th IEEE International Energy Conference (ENERGYCon)*, Gammarth, Tunisia, 2020.

[40] Said, H.A., Ringwood, J.V., Grid integration aspects of wave energy—Overview and perspectives, *IET Renewable Power Generation*, 15, 2021, 3045–3064.

[41] Mishra, R., Banerjee, U., Sekhar, T., Saha, T., Development and Implementation of Control of Stand-alone PMSG based Distributed Energy System with Variation in Input and Output Parameters, *IET Electric Power Applications*, 13, 2019, 1497-1506.

[42] Kebbati, Y., Baghli, L., Design, modeling and control of a hybrid grid-connected photovoltaic-wind system for the region of Adrar, *Algerian Journal of Environmental Science and Technology*, 20, 2023, 6531–6558.

[43] Bunjongjit, K., Kumsuwan, Y., Performance enhancement of PMSG systems with control of generator-side converter using d-axis stator current controller, *10th International Conference on Electrical Engineering/Electronics, Computer, Telecommunications and Information Technology*, Krabi, Thailand, 2013.

[44] Sikorski, A., Falkowski, P., Korzeniewski, M., Comparison of Two Power Converter Topologies in Wind Turbine System, *Energies*, 14, 2021, 6574.

[45] Mohsen, R., Modeling, control and stability analysis of grid connected PMSG based wind turbine assisted with diode rectifier and boost converter, *International Journal of Electrical Power & Energy Systems*, 93, 2017, 84-96.

[46] Fan, S., Pu, T., Liu, G., Ma, W., Li, L., Williams, B., Current output hard-switched full-bridge DC/DC converter for wind energy conversion systems, *IET Renewable Power Generation*, 8, 2014, 749-756.

ORCID iD

Ali Alnujaie https://orcid.org/0000-0003-1321-9485
Abderrahmane Berkani https://orcid.org/0000-0001-9391-786X
Karim Negadi https://orcid.org/ 0000-0002-3377-0402
Lazreg Hadji https://orcid.org/0000-0002-3333-5902
Mofareh Hassan Ghazwani https://orcid.org/0000-0002-8224-3908

Publisher's Note Shahid Chamran University of Ahvaz remains neutral with regard to jurisdictional claims in published maps and institutional affiliations.